Cruft Laboratory

Harvard University - Cambridge, Massachusetts

AN EXPERIMENTAL STUDY OF THE PROPERTIES OF ANTENNAS IMMERSED IN CONDUCTING MEDIA

By

Kenjo Iizuka and Ronold W. P. King

December 15, 1961

Scientific Report No. 2

Contract AF19(604)-7262 Project 7661, Task 76615

AFCRL-62-223

Prepared for
Geophysics Research Directorate
Air Force Cambridge Research Directorate
Office of Aerospace Research
United States Air Force
Bedford, Massachusetts

AFCRL-62-223

AN EXPERIMENTAL STUDY OF THE PROPERTIES OF ANTENNAS IMMERSED IN CONDUCTING MEDIA

by

Keigo Iizuka and Ronold W. P. King

Gordon McKay Laboratory of Applied Science

Harvard University

Cambridge, Massachusetts

Scientific Report No. 2

Contract AF19(604)-7262

December 15, 1961

Project 7661 — Task 76615

Prepared for

Geophysics Research Directorate
Air Force Cambridge Research Laboratories
Office of Aerospace Research
United States Air Force
Bedford, Massachusetts

Requests for additional copies by Agencies of the Department of Defense, their contractors, and other Government agencies should be directed to the:

ARMED SERVICES TECHNICAL INFORMATION AGENCY
ARLINGTON HALL STATION
ARLINGTON 12, VIRGINIA

Department of Defense contractors must be established for ASTIA services, or have their "need-to-know" certified by the cognizant military agency of their project or contract.

All other persons and organizations should apply to the:

U. S. DEPARTMENT OF COMMERCE
OFFICE OF TECHNICAL SERVICES
WASHINGTON 25, D. C.

SR2

AN EXPERIMENTAL STUDY OF THE PROPERTIES OF ANTENNAS IMMERSED IN CONDUCTING MEDIA

by

Keigo Iizuka and Ronold W. P. King

Cruft Laboratory, Harvard University

Cambridge, Massachusetts

Abstract

Descriptions of the apparatus for measuring both the properties of the conducting solution in which the antennas are immersed and the properties of the dipole antennas themselves, were given in Scientific Report No. 1 "Apparatus for the Study of the Properties of Antennas in a Conducting Medium" by the same authors. This report provides measured results of the driving-point admittance, the amplitude distribution of the current, and the phase distribution of the current relative to the phase at the driving point for a dipole antenna when immersed in homogeneous and inhomogeneous conducting media.

Measurements have also been made of the amplitude distribution and phase distribution of the current for a half-wave dipole antenna immersed in a stratified medium for various gradients of the conductivity. The results of these experiments indicate that either an antenna of short electrical length or a half-wave dipole antenna can be used as a probe to measure the dielectric constant and conductivity of the medium in which it is immersed. A half-wave dipole antenna could well be used to detect an inhomogeneity in an extended medium.

1. Introduction

The properties of dipole antennas when immersed in a conducting medium are currently of interest, not only from theoretical but also from practical points of view. A knowledge of the characteristics of an antenna immersed in such a medium may have applications in determining the properties

of ionized gases, in under-water communications and in geophysical explorations. The studies were made on single antennas of moderate length in a homogeneous dissipative medium and also in media with properties that were stratified in layers perpendicular to the antenna.

In homogeneous media, measurements of the driving-point admittance have been made for a range of values of the ratio $\frac{\sigma}{\omega\epsilon_r\epsilon_o}$ of the medium taking the electrical height of the antenna βh as a parameter. The ratio $\frac{\sigma}{\omega\epsilon_r\epsilon_o}$ is varied from $\frac{\sigma}{\omega\epsilon_r\epsilon_o} = 0.0356$ to $\frac{\sigma}{\omega\epsilon_r\epsilon_o} = 8.8$ and the antenna height βh is varied from $\beta h = 0.1$ to 2π at intervals of 0.1. The amplitude and phase distributions of the current have been measured for $\beta h = \pi/4$, $\pi/2$, $3\pi/4$, π , $5/4\,\pi$, $3/2\,\pi$, $7/4\,\pi$, and 2π in a homogeneous conducting medium whose conductivity is varied from $\frac{\sigma}{\omega\epsilon_r\epsilon_o} = 0.036$ to $\frac{\sigma}{\omega\epsilon_r\epsilon_o} = 8.8$.

In stratified media, measurements have been made of the amplitude and phase distributions of the current and of the driving-point admittance for a half-wave dipole antenna in a tank that is stratified in layers perpendicular to the antenna by thin nylon separators. The conductivity of the solutions in the layers was varied linearly with respect to the distance from the driving-point of the dipole antenna.

II. Experimental Arrangements

Descriptions of the measuring equipment and the tank for use with homogeneous media are in an earlier report.[1] A description of the stratification of the tank follows. The tank was divided into seven layers parallel to the image plane and consisting of solutions of different conductivity and dielectric constant. Nylon film 0.004" thick was stretched over a plastic frame. Six such framed nylon sheets were used to divide the tank into seven watertight compartments. Photographs of the structure and the dimensions of the compartments are shown in Figs. 3-21 and 3-22. The layers consist of five small and two relatively large compartments. The first five are located nearer the image plane; they have equal dimensions and the thickness of the layer is $2/9$ the length of a half-wave dipole antenna. At about one-third of the distance between the small compartments and the back wall another nylon sheet is placed to separate the sixth from the seventh compartment.

III. Experimental Results

A. With Homogeneous Medium

Driving-point admittance

The measuring procedure utilizes the height of the antenna and the properties of the homogeneous solution in which the antenna is immersed as variables.

The driving-point admittance was measured for the range from $\beta h = 0.1$ to $\beta h = 2\pi$ at intervals of $\beta h = 0.1$. The properties of the solution were varied from $\epsilon_r = 78$, $\sigma/\omega\epsilon_r\epsilon_o = 0.036$ to $\epsilon_r = 69$, $\sigma/\omega\epsilon_r\epsilon_o = 8.8$. The measured results are plotted on the rectangular admittance chart taking the length of the antenna βh as a parameter. These rectangular admittance charts are in Fig. 3-1 through Fig. 3-10 with various ϵ_r and $\sigma/\omega\epsilon_r\epsilon_o$ values. The values of ϵ_r and $\sigma/\omega\epsilon_r\epsilon_o$ which belong to the curves are indicated in the figures.

As a general characteristic of the curves, note that the size of the spiral curves gets smaller, i.e., the spacing between the neighboring circumferences becomes smaller and the convergence of the spiral with respect to βh becomes faster as $\sigma/\omega\epsilon_r\epsilon_o$ is increased.

The point of convergence of the spiral moves from the capacitive region into the inductive region as the value of $\sigma/\omega\epsilon_r\epsilon_o$ is increased. This may be better understood from Fig. 3-11. The change in the admittance of the antenna with an increase in the conductivity of the solution for βh values of 0.3, $\frac{\pi}{4}$, $\frac{\pi}{2}$, $\frac{3}{4}\pi$, π, $\frac{5}{4}\pi$, $\frac{3}{2}\pi$, and 2π are shown. In this figure a large spiral curve, which was measured with the lowest conductivity, is also plotted as a reference.

Starting from the values on the spiral, the admittance values move in the general direction of higher conductance and larger negative susceptance as the conductivity is increased. It is interesting to note that all loci except for antennas shorter than $\beta h = \pi/2$ first meet near the point $Y = 28 - j3$ millimho which is not far from the characteristic admittance of the line

$Y_c = 20.87$ millimho, and then these move together toward the larger values of conductance and susceptance as the conductivity of the solution is increased further. The loci from the meeting point on are practically the same regardless of the lengths of the antenna; the conductivity of the solution at the meeting point is $\sigma/\omega\epsilon_r\epsilon_o = 1.06$ for all the antenna lengths. This behavior is observed because in the solutions with the higher conductivities most of the charges leak away from the antenna into the solution and the magnitude of the current greatly decreases outward from the driving point. The contribution by the current farther than a certain βz value to the driving-point admittance is negligible. This certain point may be set to be near $\beta h = \pi/2$ since the antennas shorter than this length do not quite follow the same loci.

The measured admittance of an antenna with smaller radius and without the penton cover (Fig. 2-29 of Scientific Report No. 1), follows practically the same kind of locus. The broken line in Fig. 3-11 represents the results with the thinner antenna. The above-mentioned facts can be better seen by replotting the admittance in rectangular coordinates as a function of βh. The conductance G as a function of the antenna length βh is plotted in Fig. 3-12; the corresponding susceptance β in Fig. 3-13 . It is noted that as the value of the parameter $\sigma/\omega\epsilon_r\epsilon_o$ increases the oscillations in the amplitude of both the conductance and the susceptance curves become flatter and both G and B go into a region of monotonic increase where the effect of the conductivity of the solution in which the driving point is immersed affects the admittance more than does the length of the antenna. The resonance condition disappears when the length of the antenna exceeds $\beta h = \pi$ in the solution of higher conductivity since the susceptance stays in the inductive region. It should also be noticed that the resonance points shift toward the origin as $\sigma/\omega\epsilon_r\epsilon_o$ is increased more than would be expected from the increase in the value of β (which is a function of $\sigma/\omega\epsilon_r\epsilon_o$ referring to Eq. 1.3 of Scientific Report No. 1 .

The change in the driving-point admittance of an antenna of fixed length with an increase in the conductivity of the solution may be discussed with reference to Fig. 3-11 . As was mentioned before, the admittances of the antennas longer than $\beta h = \pi/2$ first move toward the common junction point and then all go to higher G and $|B|$ values together. By examining the loci

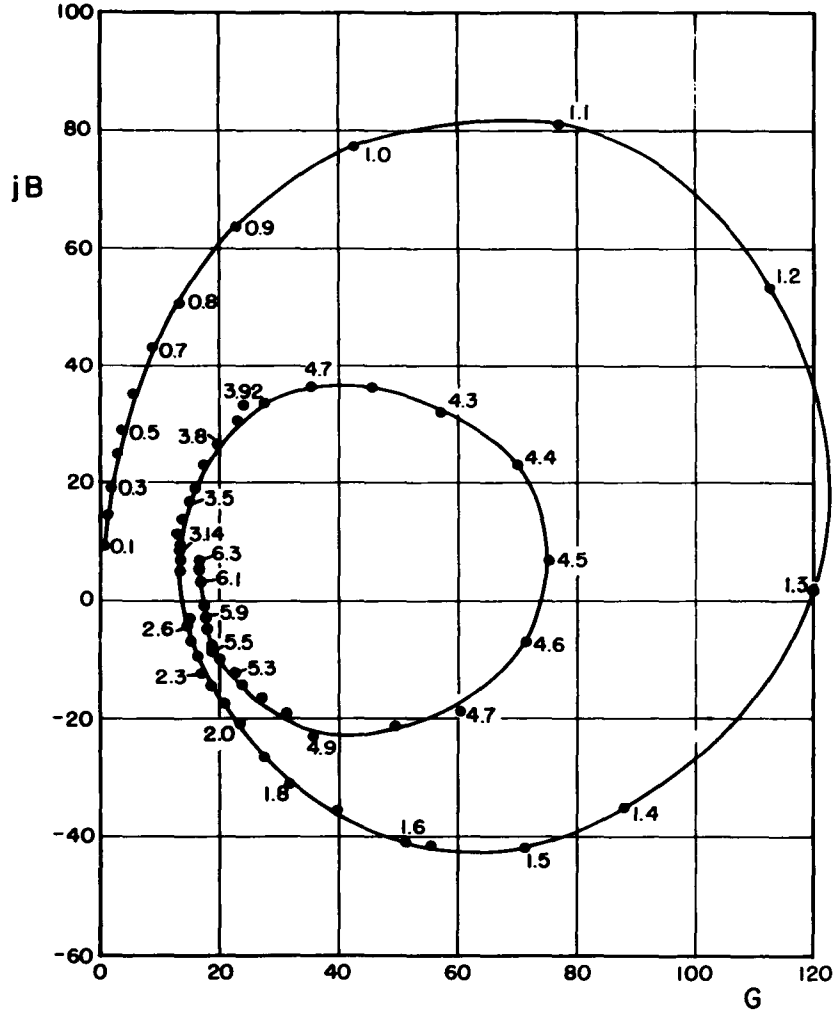

FIG. 3-1 MEASURED ADMITTANCE IN THE SOLUTION WITH $\epsilon_r = 78$, $\frac{\sigma}{\omega \epsilon_r \epsilon_0} = 0.036$

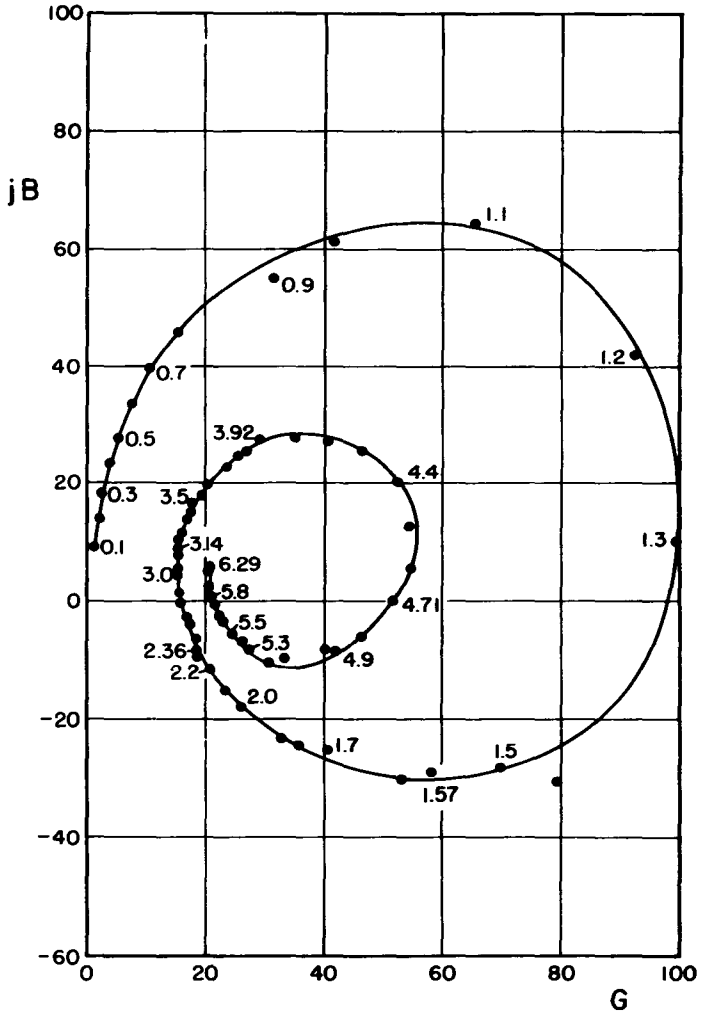

FIG. 3-2 MEASURED ADMITTANCE IN THE SOLUTION WITH $\epsilon_r = 78$ $\frac{\sigma}{\omega \epsilon_r \epsilon_0} = 0.088$

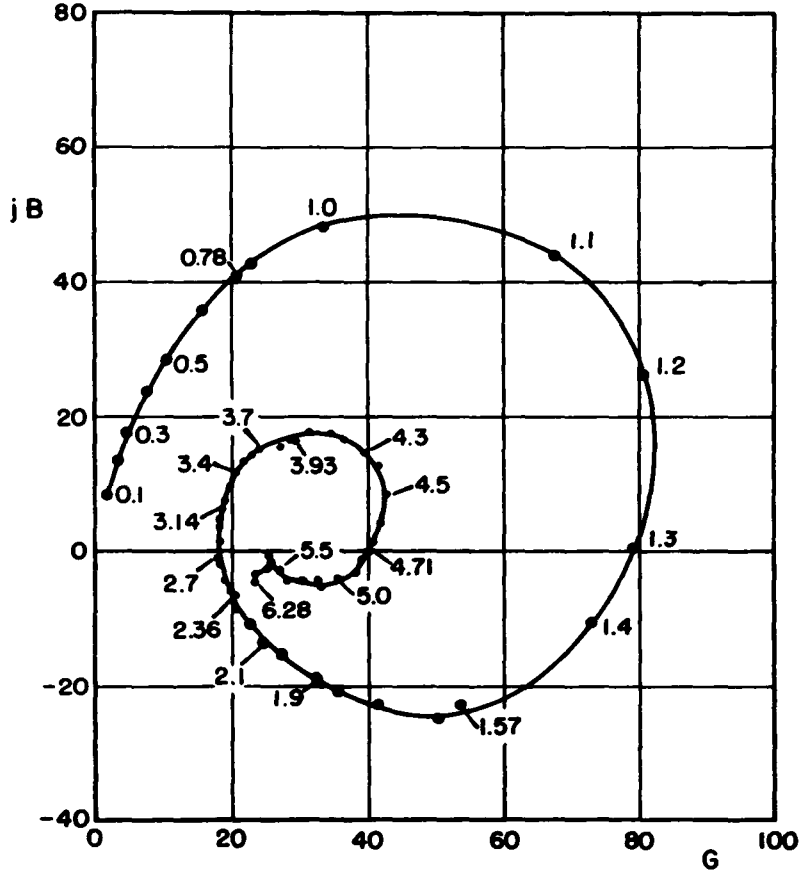

FIG. 3-3 MEASURED ADMITTANCE IN THE SOLUTION WITH $\epsilon_r = 78$ $\frac{\sigma}{\omega \epsilon_r \epsilon_0} = 0.18$

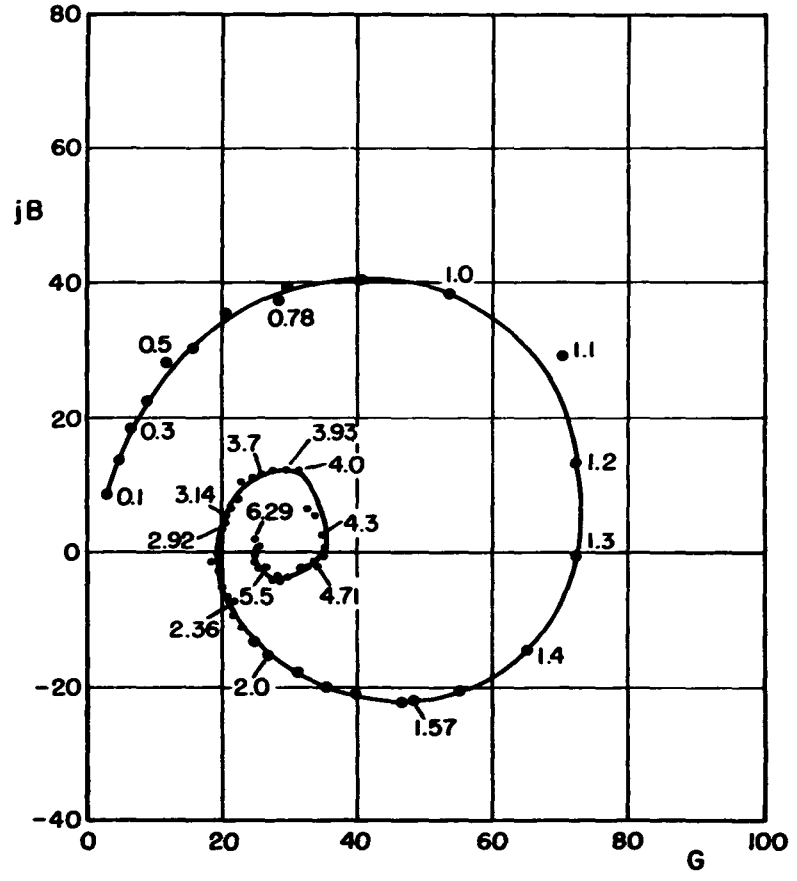

FIG. 3-4 MEASURED ADMITTANCE IN THE SOLUTION WITH $\epsilon_r = 78$, $\frac{\sigma}{\omega \epsilon_r \epsilon_0} = 0.35$

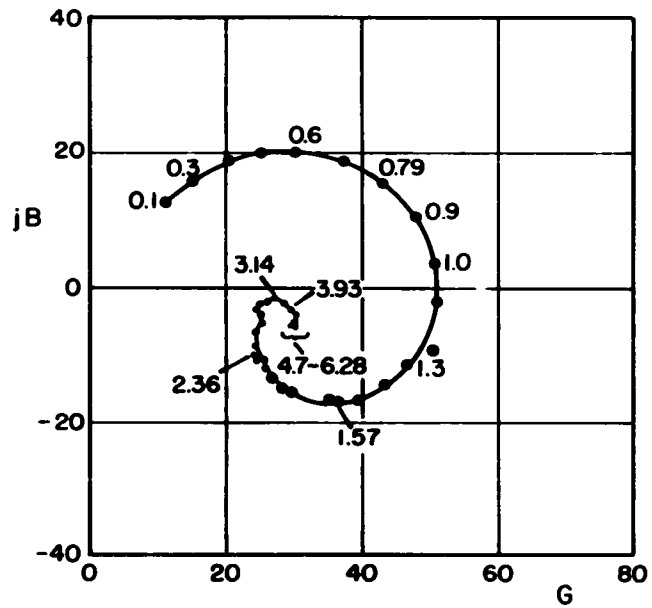

FIG. 3-5 MEASURED ADMITTANCE IN THE SOLUTION WITH $\epsilon_r = 78$, $\frac{\sigma}{\omega \epsilon_r \epsilon_0} = 0.53$

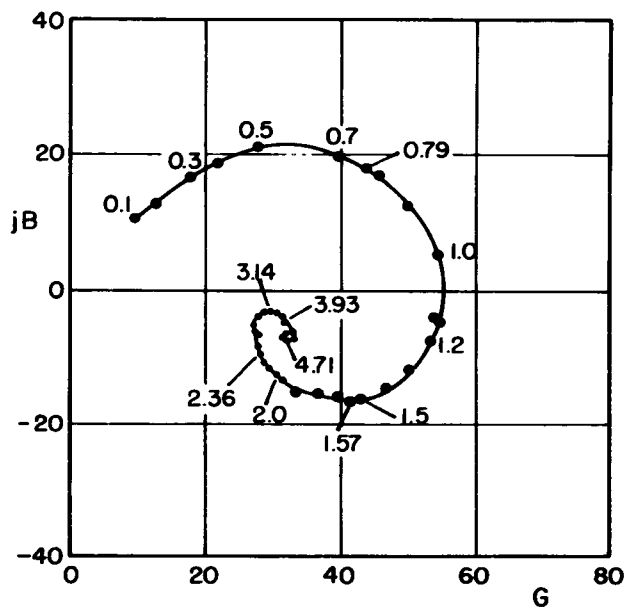

FIG. 3-6 MEASURED ADMITTANCE IN THE SOLUTION WITH $\epsilon_r = 77$, $\frac{\sigma}{\omega \epsilon_r \epsilon_0} = 1.06$

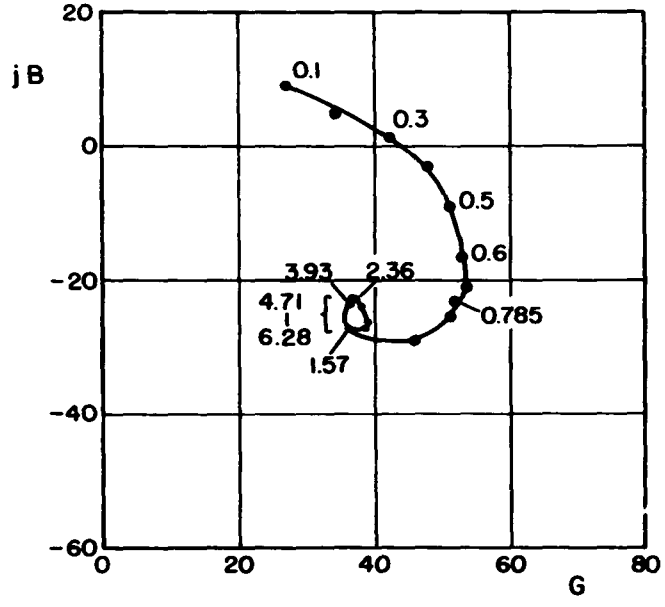

FIG. 3-7 MEASURED ADMITTANCE IN THE SOLUTION WITH $\epsilon_r = 74$, $\frac{\sigma}{\omega \epsilon_r \epsilon_0} = 2.64$

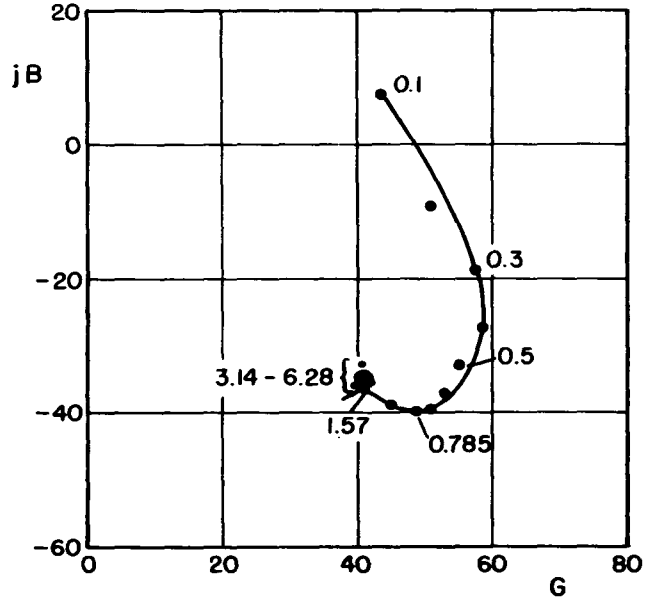

FIG. 3-8 MEASURED ADMITTANCE IN THE SOLUTION WITH $\epsilon_r = 72$, $\frac{\sigma}{\omega \epsilon_r \epsilon_0} = 4.40$

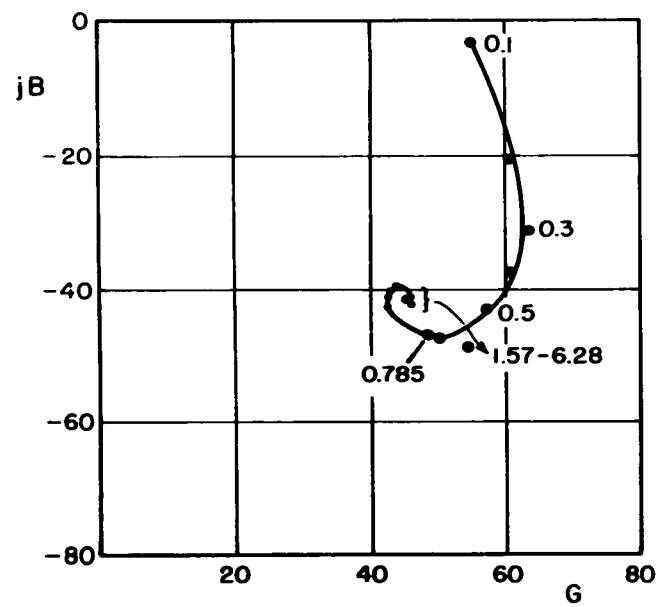

FIG. 3-9 MEASURED ADMITTANCE IN THE SOLUTION WITH $\epsilon_r = 70$, $\frac{\sigma}{\omega \epsilon_r \epsilon_0} = 6.20$

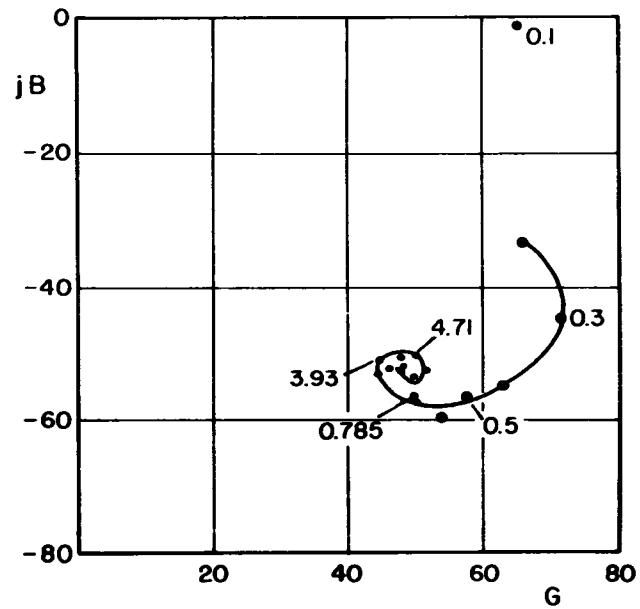

FIG. 3-10 MEASURED ADMITTANCE IN THE SOLUTION WITH $\epsilon_r = 69$, $\frac{\sigma}{\omega \epsilon_r \epsilon_0} = 8.80$

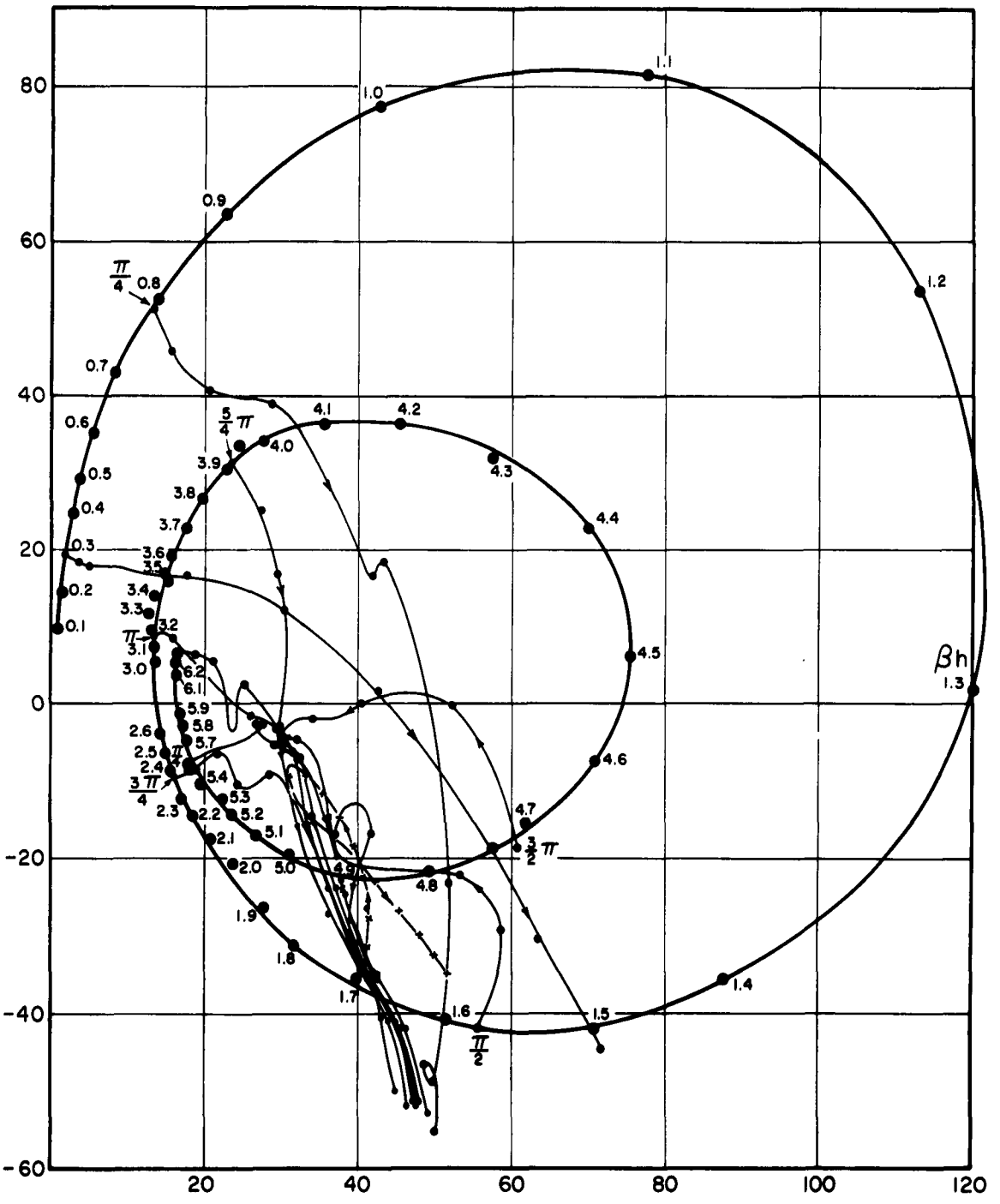

FIG. 3-11 LOCI OF ADMITTANCE WITH THE CHANGE OF CONDUCTIVITY

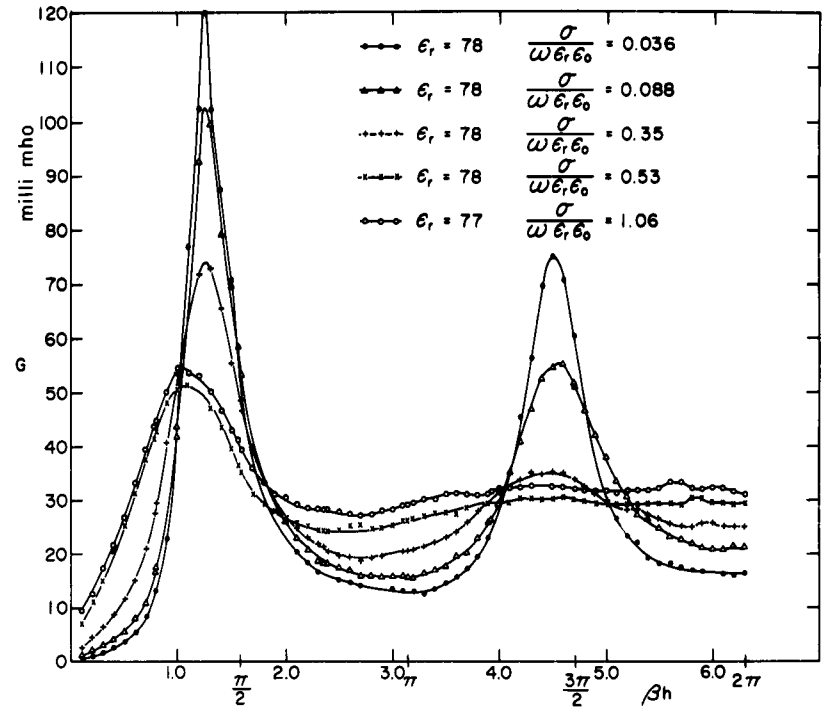

FIG. 3-12 DRIVING-POINT CONDUCTANCE VERSUS ANTENNA LENGTH

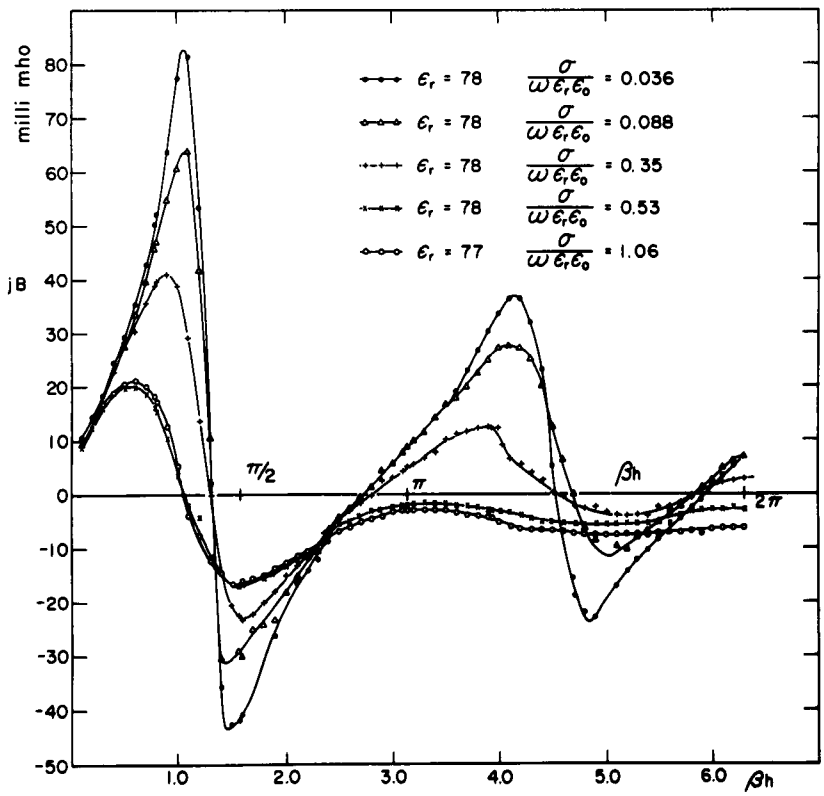

FIG. 3-13 DRIVING-POINT SUSCEPTANCE VERSUS ANTENNA LENGTH

closely, their behavior can be summarized in the following two statements :

(1) The loci almost without exception select the most direct path to the common meeting point.

(2) As a consequence of (1), the shapes of the driving-point admittance curves for a fixed wavelength with respect to the conductivity of the solution may be classified as follows :

a) For antenna lengths lying below and to the right of the meeting point on the chart, both G and $|B|$ curves have minima i.e.,

$$\left.\begin{array}{l} \frac{\pi}{2} < \beta h < 1.8 \\ 4.6 < \beta h < 5.0 \end{array}\right\} \text{ both G and } |B| \text{ have minima.}$$

b) For antenna lengths lying below and to the left of the meeting point G does not have minima while $|B|$ does

$$\left.\begin{array}{l} 1.9 < \beta h < 2.6 \\ 5.1 < \beta h < 5.7 \end{array}\right\} \begin{array}{l} \text{G does not have minima} \\ |B| \text{has minima.} \end{array}$$

c) For antenna lengths lying above and to the left of the meeting point neither G nor $|B|$ has minima

$$\left.\begin{array}{l} 0.1 < \beta h < 0.9 \\ 2.7 < \beta h < 4.0 \\ 5.8 < \beta h < 2\pi \end{array}\right\} \text{ neither G nor } |B| \text{ has minima.}$$

d) For antenna lengths lying above and to the right of the meeting point G has minima while B does not have minima

$$\left.\begin{array}{l} 1.0 < \beta h < 1.3 \\ 4.1 < \beta h < 4.5 \end{array}\right\} \begin{array}{l} \text{G has minima; B does not} \\ \text{have minima.} \end{array}$$

It may be said that from the viewpoint of the application of the dipole antenna to the measurement of the properties of the medium, it might be better to select an antenna length which does not have extrema, for if the curve

has extrema it has more than one value of $\sigma/\omega\epsilon_r\epsilon_o$ corresponding to the same driving-point conductance (or susceptance). The antenna lengths in the group (c) seem to be most suitable for this type of application.

The verification of the above classification can be best seen from the curve of the driving-point conductance with respect to the value of $\sigma/\omega\epsilon_r\epsilon_o$ in Fig. 3-14 and the driving-point susceptance with respect to the value of $\sigma/\omega\epsilon_r\epsilon_o$ in Fig. 3-15. Here the experimental result with a short antenna ($\beta h = 0.3$) is compared with the available theoretical results [1]. Even though it is not quite possible to compare the measured value with the numerically calculated results due to the difference in Ω and the presence of the penton tubing on the antenna, the general shape of both experimental and theoretical curves are quite alike. The conductance curve increases in a fairly linear manner with an increase in the conductivity; it is concave upwards in the region of high conductivities. The susceptance curve decreases relatively slowly with an increase in conductivity and changes its sign at higher conductivities as the theoretical result does.

Current Distribution

The amplitude and relative phase distributions of the current were measured for antennas with $\beta h = \pi/4$, $\pi/2$, $3\pi/4$, and π in the solutions $\epsilon_r = 78\ \sigma/\omega\epsilon_r\epsilon_o = 0.036$, $\epsilon_r = 78\ \sigma/\omega\epsilon_r\epsilon_o = 0.35$, $\epsilon_r = 77\ \sigma/\omega\epsilon_r\epsilon_o = 1.06$, $\epsilon_r = 74\ \sigma/\omega\epsilon_r\epsilon_o = 2.6$, $\epsilon_r = 69\ \sigma/\omega\epsilon_r\epsilon_o = 8.8$. The measured results are plotted in Figs. 3-16 through 3-19 . The amplitude of the current along the antenna is normalized to the value of $Y = \frac{|I(0)|}{V}$ ma/volt. The phase of the current along the antenna is referred to $\theta_I(0) = \tan^{-1}\frac{B}{G}$ $(= \tan^{-1}\frac{I'(0)}{I''(0)})$.

It is observed from this set of curves that for all lengths of antenna the current distribution nearer the tip of the antenna begins first to change from concave outward to concave inward, and then that nearer the base of the antenna does the same as $\sigma/\omega\epsilon_r\epsilon_o$ is increased. The shape of I'' (current component in phase with the driving-point voltage) in general suffers more from this change of curvature than that of I' (current component 90 degrees out of phase with the driving-point voltage) with an increase in $\sigma/\omega\epsilon_r\epsilon_o$. With an increase in conductivity the curve of θ_I becomes straighter and the shape

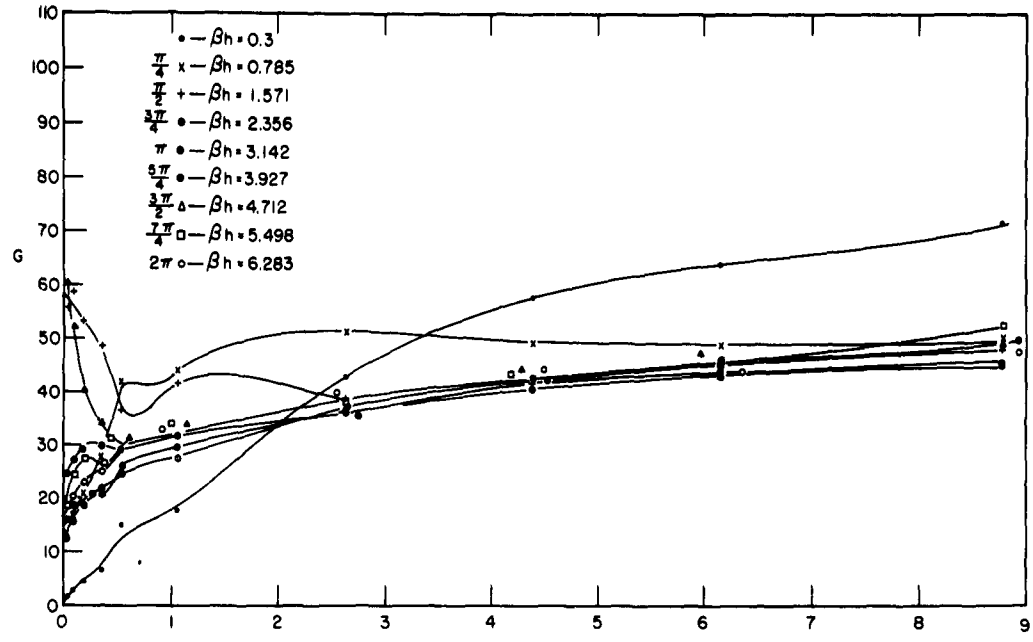

FIG. 3-14 DRIVING-POINT CONDUCTANCE VERSUS $\frac{\sigma}{\omega \epsilon_r \epsilon_0}$

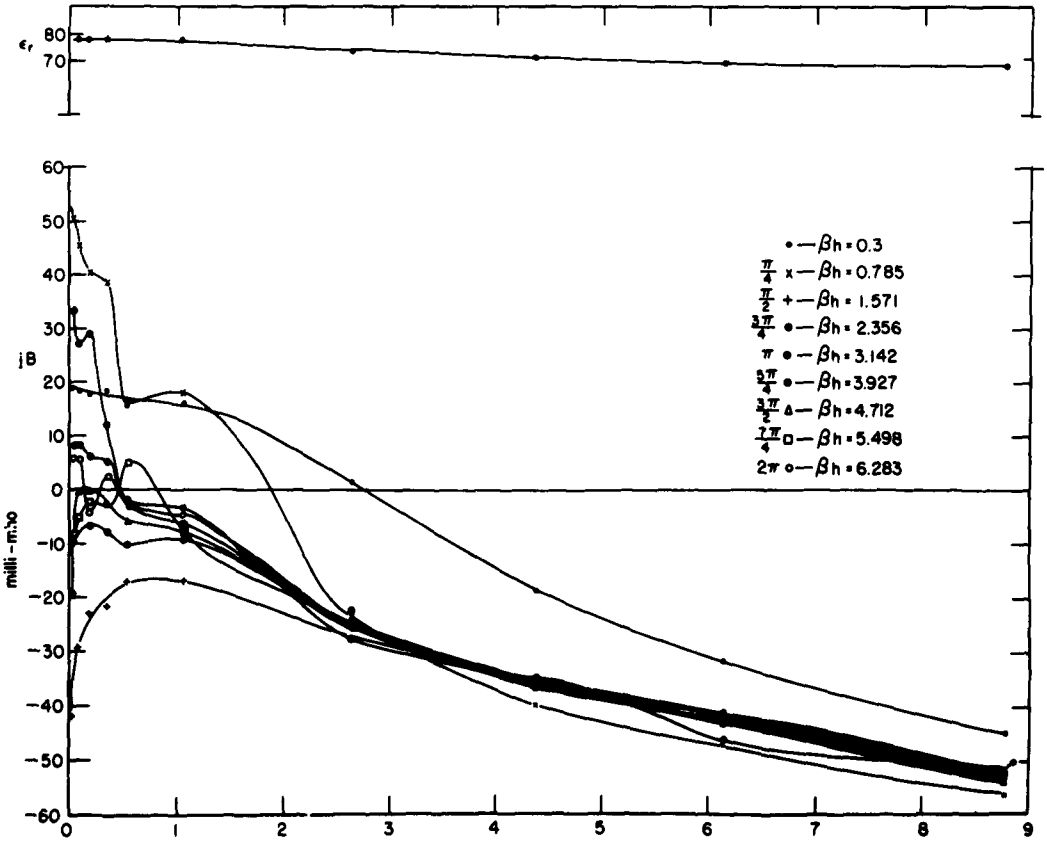

FIG. 3-15 DRIVING-POINT SUSCEPTANCE VERSUS $\frac{\sigma}{\omega \epsilon_r \epsilon_0}$

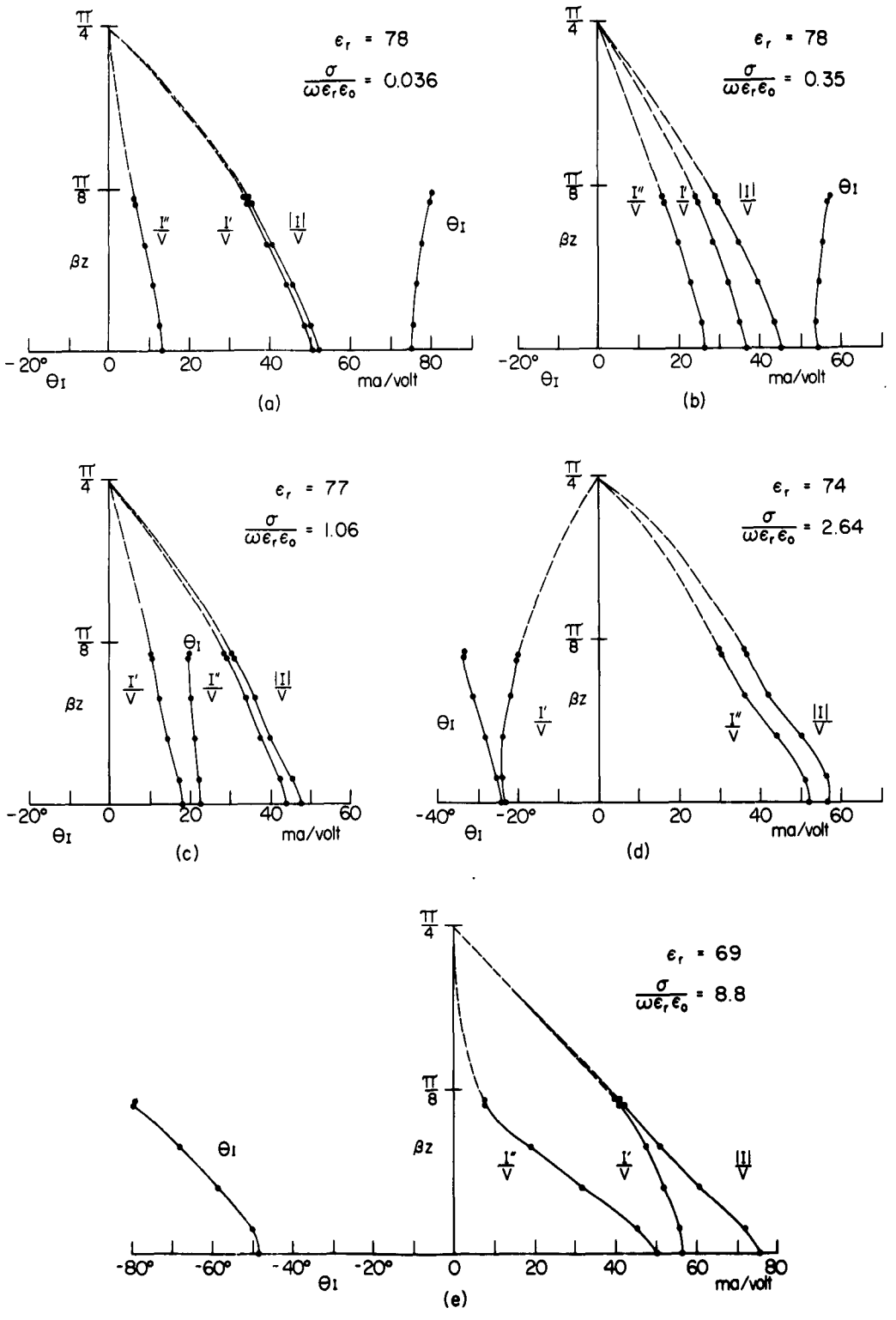

FIG. 3-16 CURRENT DISTRIBUTION $\frac{I}{V} = \frac{|I|}{V} e^{j\theta_I} = \frac{I''}{V} + j\frac{I'}{V}$ ALONG AN ANTENNA WITH $\beta h = \frac{\pi}{4}$ IN VARIOUS SOLUTIONS.

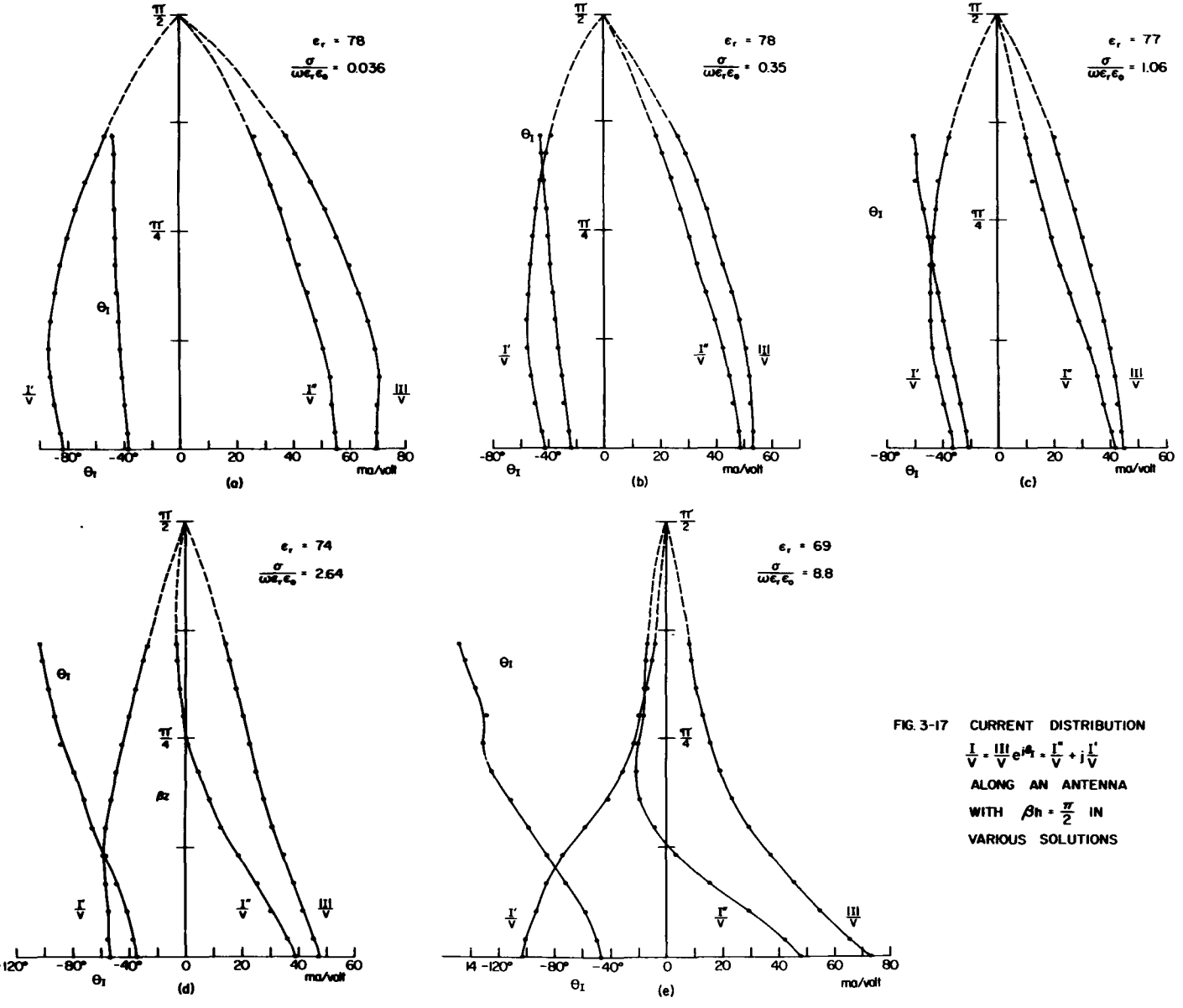

FIG. 3-17 CURRENT DISTRIBUTION $\frac{I}{V} = \frac{III}{V} e^{i\phi_I} = \frac{I''}{V} + j\frac{I'}{V}$ ALONG AN ANTENNA WITH $\beta h = \frac{\pi}{2}$ IN VARIOUS SOLUTIONS

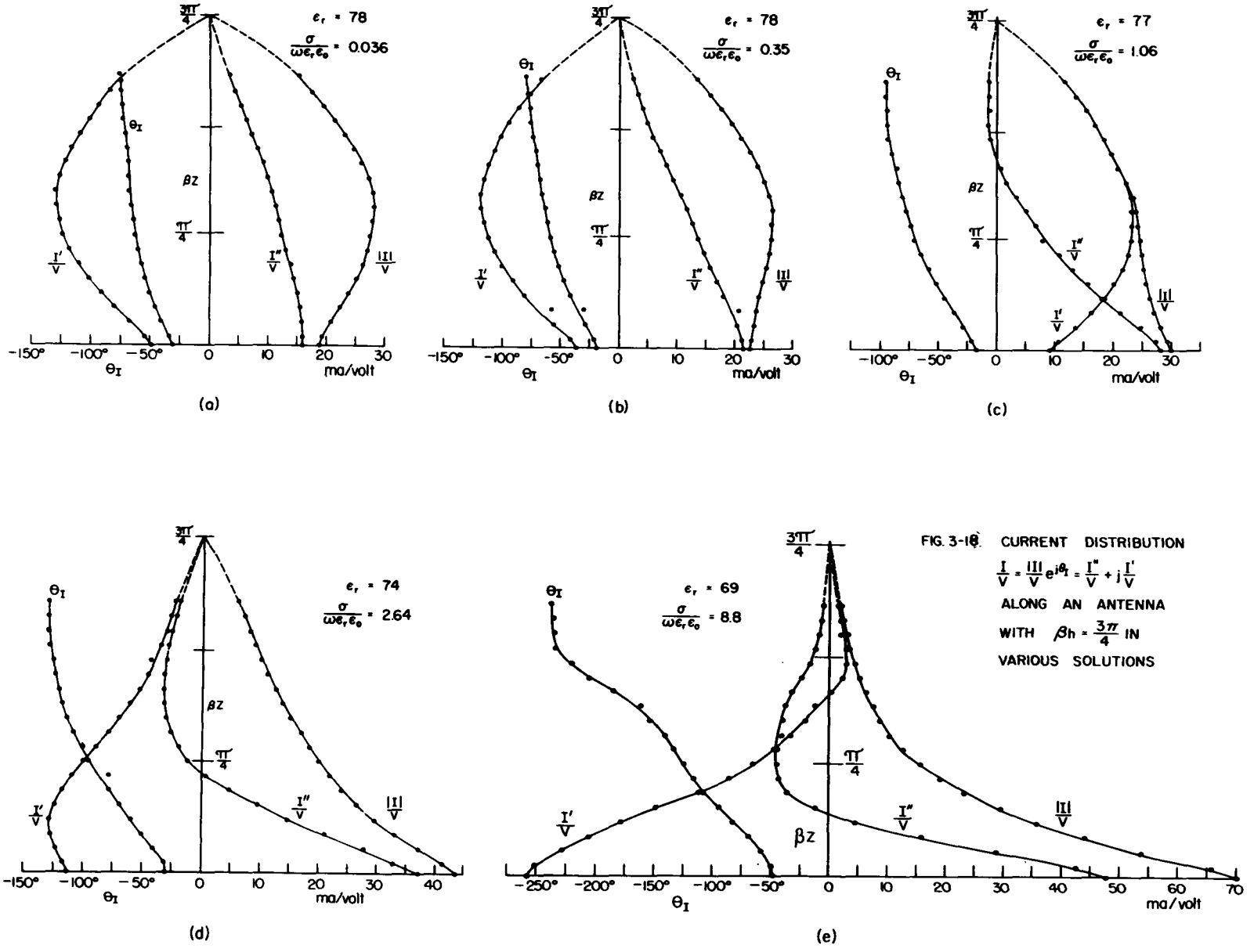

FIG. 3-18. CURRENT DISTRIBUTION $\frac{I}{V} = \frac{|I|}{V} e^{j\theta_I} = \frac{I''}{V} + j\frac{I'}{V}$ ALONG AN ANTENNA WITH $\beta h = \frac{3\pi}{4}$ IN VARIOUS SOLUTIONS

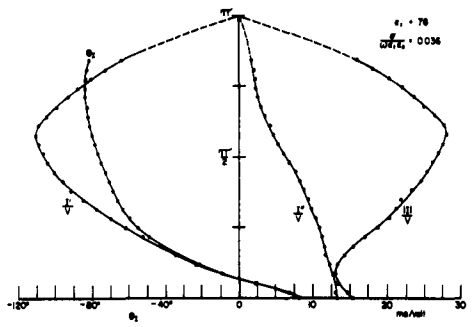

(a)

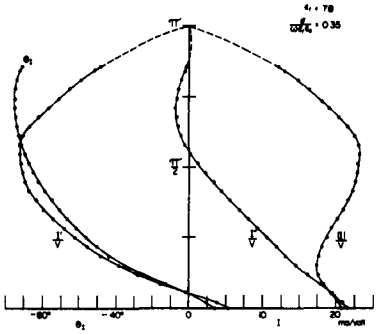

(b)

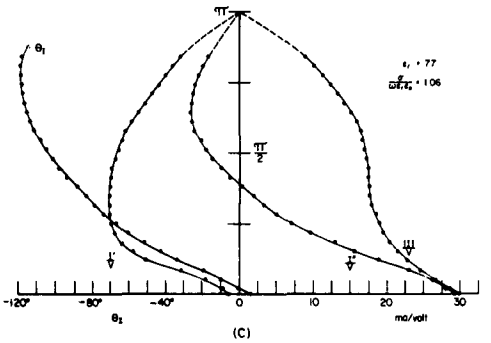

(C)

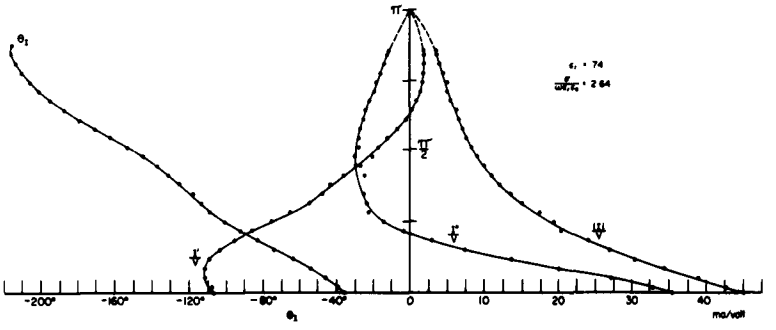

(d)

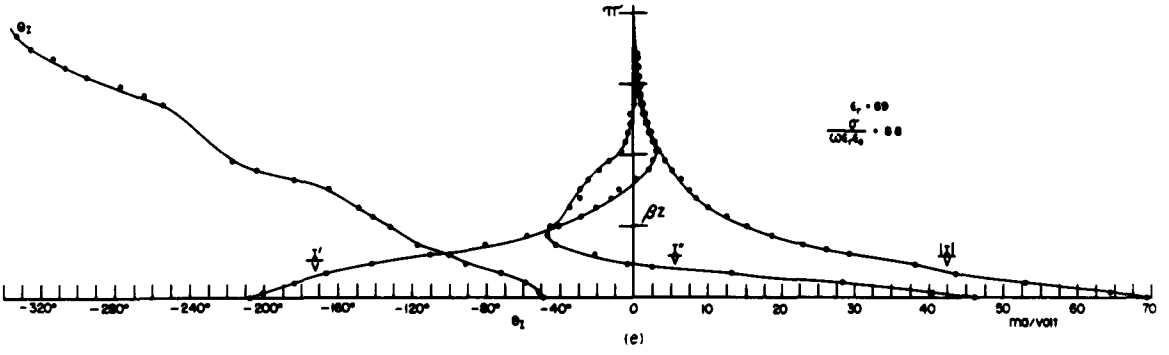

(e)

FIG 3-19 CURRENT DISTRIBUTION $\frac{1}{2}V = \frac{1}{2}V e^{j\theta_2} = I' + j\,I''$ ALONG AN ANTENNA WITH $\beta h = \pi$ IN VARIOUS SOLUTIONS

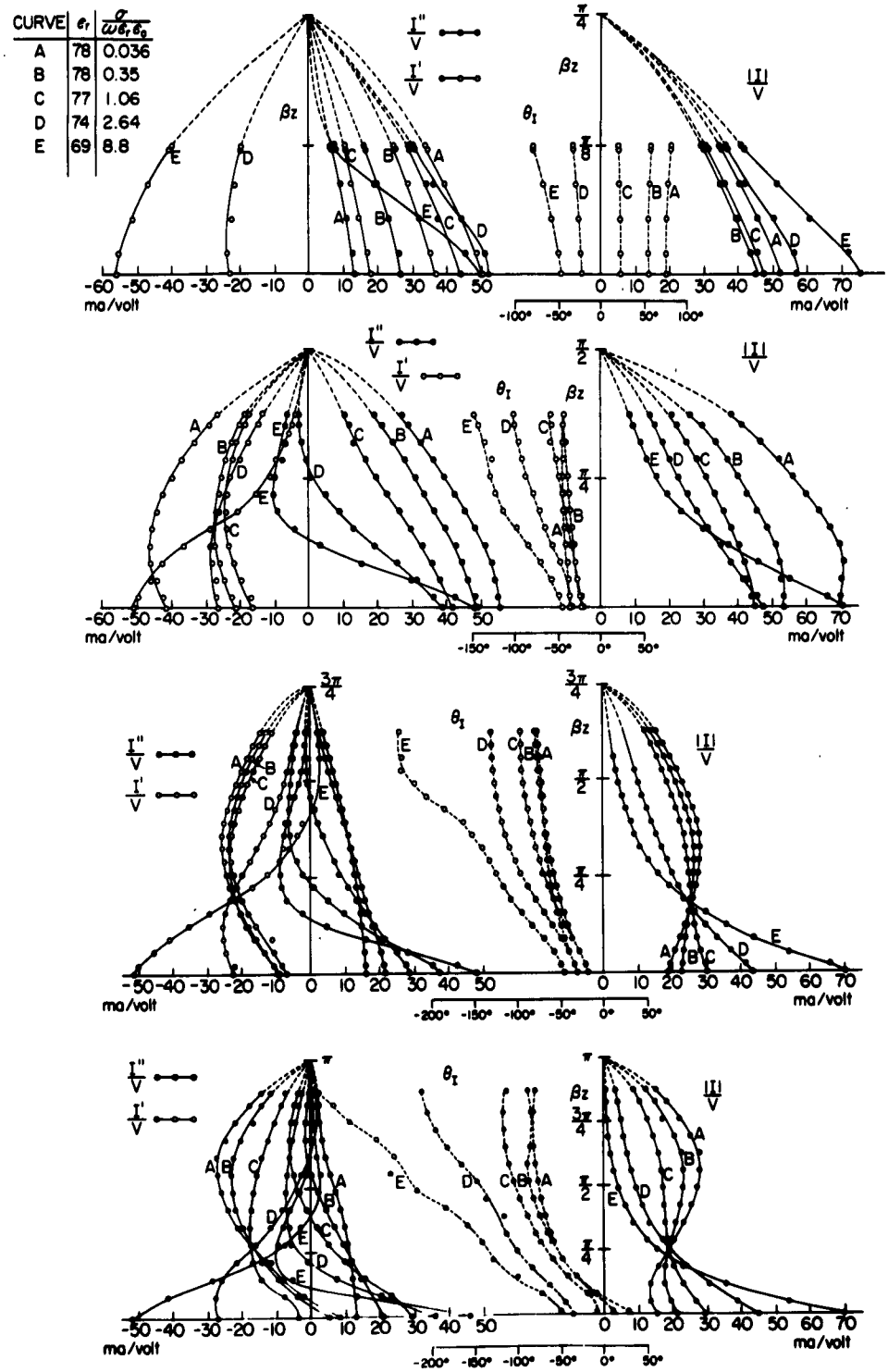

FIG. 3-19(a) CURRENT DISTRIBUTION $\frac{I}{V} = \frac{III}{V} e^{j\theta_I} = \frac{I''}{V} + j\frac{I'}{V}$ ALONG ANTENNAS $\beta h = \frac{\pi}{4}, \frac{\pi}{2}, \frac{3\pi}{4}, \pi$ IN SOLUTIONS WITH VARIOUS CONDUCTIVITIES.

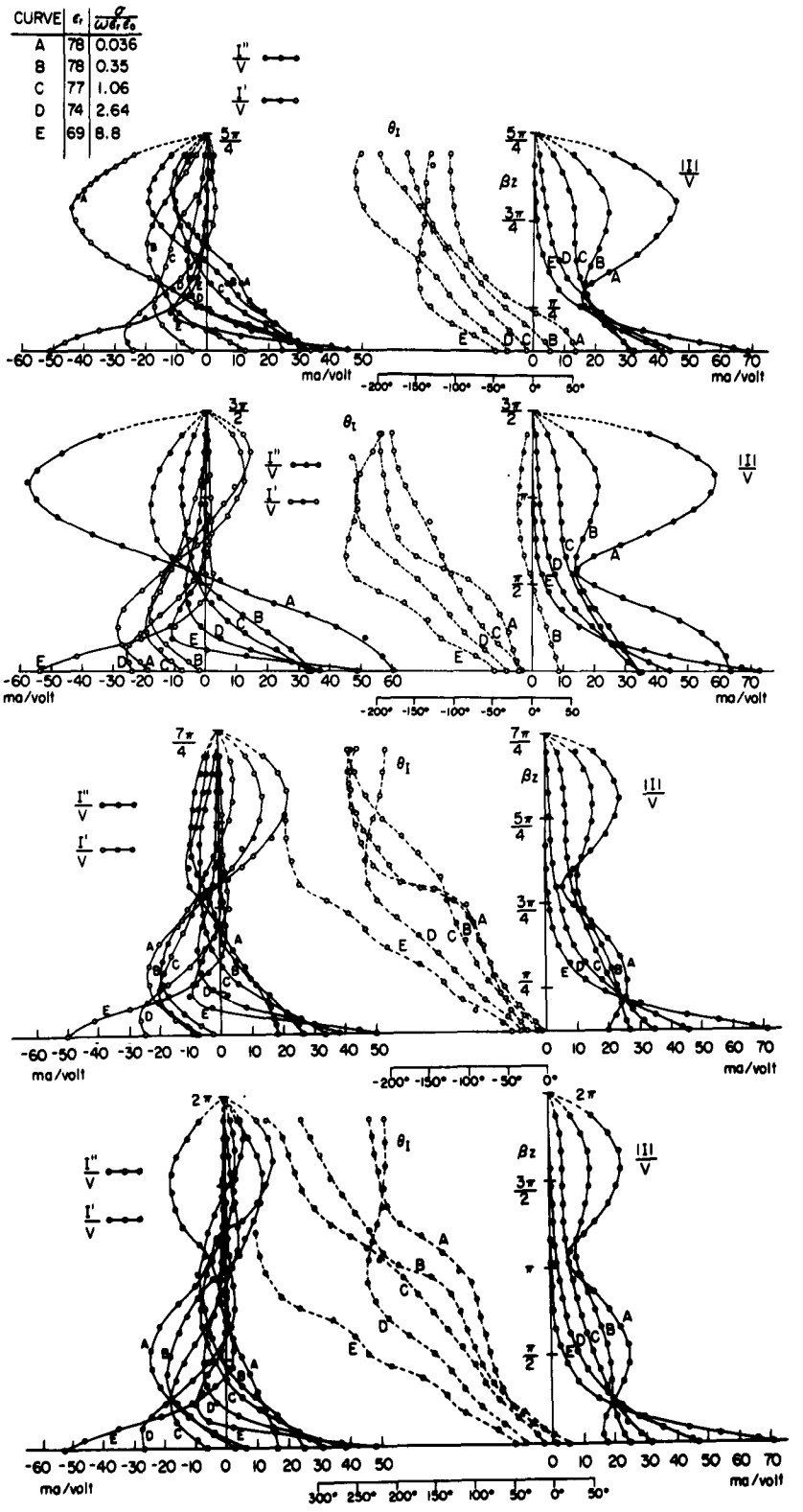

FIG. 3-19(b) CURRENT DISTRIBUTION $\frac{I}{V} = \frac{|I|}{V} e^{j\theta_I} = \frac{I''}{V} + j\frac{I'}{V}$ ALONG ANTENNAS $\beta h = \frac{5\pi}{4}, \frac{3\pi}{2}, \frac{7\pi}{4}, 2\pi$ IN SOLUTIONS WITH VARIOUS CONDUCTIVITIES.

of the curve becomes more like that of the traveling wave linear antenna [2]. It is also noticed that the slope of the θ_I curve as a function of the position along the antenna becomes steeper just as if the electrical length of the antenna were increased, with an increase in conductivity of the solution. This trend coincides with the fact discussed in the previous section that the curves of the driving-point admittance as a function of βh shift as if the length of the antenna became longer than the physical dimension (see Figs. 3-12 through 3-13) with an increase in $\sigma/\omega\epsilon_r\epsilon_o$ value.

As for a short antenna, its current distribution becomes very close to the shape of a triangle at high conductivities of the solution. The theoretical current distribution for an antenna with $\beta h = \pi/2$ is available in references 1 and 3 and the shapes of both theoretical and measured curves are quite alike.

The amplitude of the current nearer the tip of antennas longer than $\beta h = \pi/2$ usually becomes very small for values of $\sigma/\omega\epsilon_r\epsilon_o$ that are larger than unity in comparison with that at the base of the antenna. It may be added that this fact contributes to the existence of the meeting point in the admittance chart discussed in the previous section.

In order to make a closer comparison between the current distribution of the antenna of the same height with different $\frac{\sigma}{\omega\epsilon_r\epsilon_o}$ values, the current distribution curves were replotted in Fig. 3-19(a) and Fig. 3-19(b).

It is interesting to note that the absolute values of the current near $\beta z = \frac{\pi}{4}$ are always $\left|\frac{I}{V}\right| \sim 20$ to 25 $^{ma}/_{V}$, that is, for all lengths of the antenna the current $\left|\frac{I}{V}\right|$ near $\beta z = \frac{\pi}{4}$ is approximately independent of the conductivity of the solution in the range from $\frac{\sigma}{\omega\epsilon_r\epsilon_o} = 0.036$ to 8.8. A picture of a space model of the current with various $\sigma/\omega\epsilon_r\epsilon_o$ values is shown in Fig. 3-20.

B. With Inhomogeneous Medium

Driving-Point Admittance

Before any measurements were made the effect of the presence of the films on the driving-point admittance was determined. The driving-point admittance of a half-wave dipole immersed in a homogeneous solution with $\epsilon_r = 78$ and

$\sigma/\omega\epsilon_r\epsilon_o = 0.036$ is $Y = 55.31 - j41.95$ millimho, while that of the half-wave dipole immersed in the same solution but with the presence of partition films is $Y = 52.70 - j38.8$ millimho. The difference is less than $7 \sim 8$ percent and the effect of the presence of the film on the driving-point admittance is small.

The driving-point admittance was measured for various combinations of b and S in

$$\frac{\sigma}{\omega\epsilon_r\epsilon_o} = b + Sx \quad (x \text{ in cm}) \qquad (3.1)$$

The origin of the coordinates is taken at the driving-point of the dipole antenna and the x-axis is taken along the antenna. The conductivity of the solution is changed stepwise and the geometric centers of each layer follow the distribution expressed by Eq. 3.1. Three different values of +S were taken for each of the four different b values totaling twelve different combinations of b and +S. Besides these, two -S values were also taken.

	b	S/cm		b	S/cm
0	0.036	0	8	0.70	0.096
1	0.036	0.032	9	0.70	0.16
2	0.036	0.096	10	1.06	0.032
3	0.036	0.16	11	1.06	0.096
4	0.18	0.032	12	1.06	0.16
5	0.18	0.096	13	0.30	-0.032
6	0.18	0.16	14	0.90	-0.096
7	0.70	0.032			

Table 3-11 Combinations of b and S

The measured admittances with these fourteen combinations were plotted in terms of b - S coordinates and equi-conductance and equi-susceptance contours were drawn as shown in Fig. 3-23 and Fig. 3-24 respectively. The equi-admittance curves are rather irregular and it is a hard task to give a generally significant description.

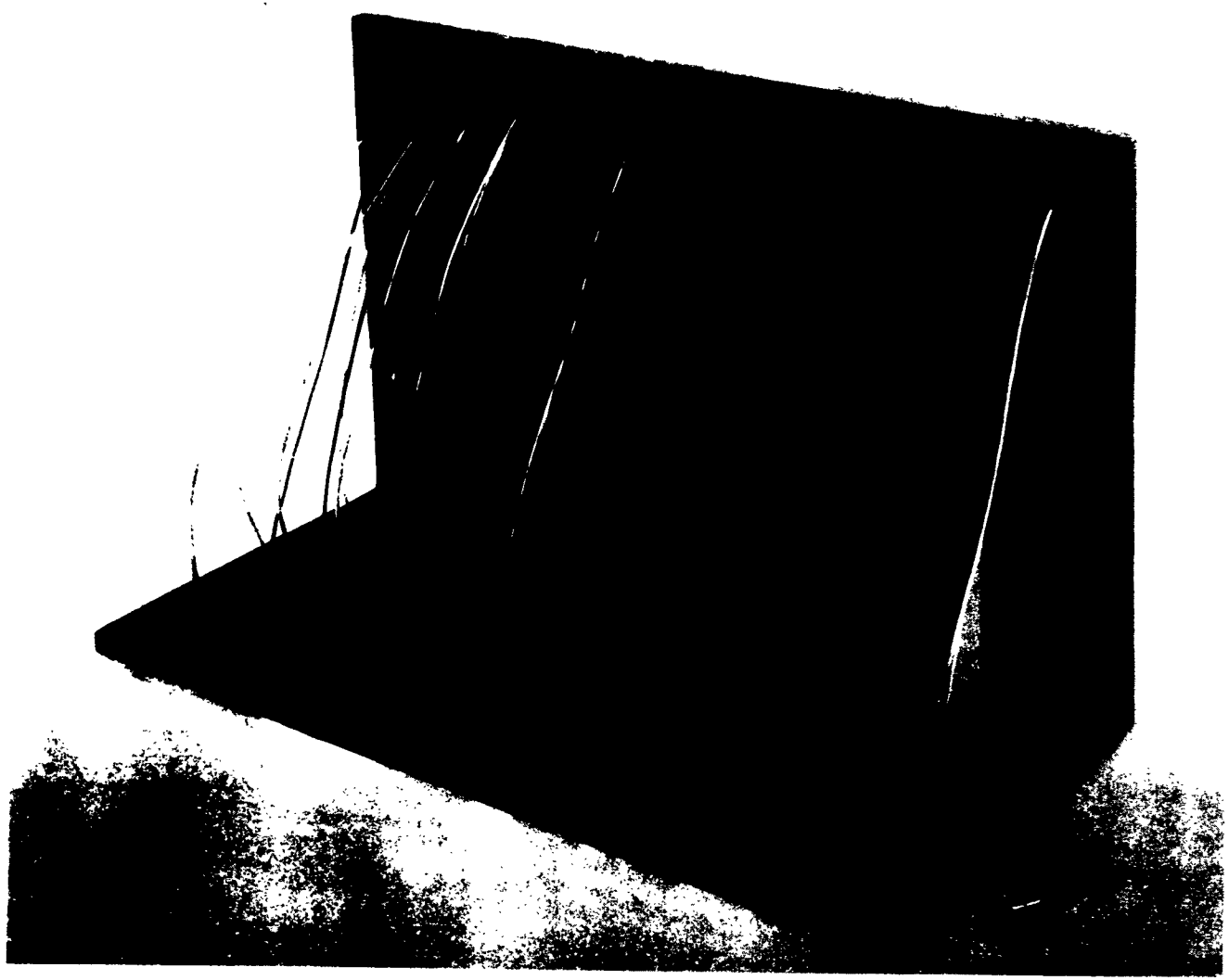

FIG. 3-20 PHOTO OF A SPACE MODEL OF THE CURRENT DISTRIBUTION ALONG A HALF-WAVE DIPOLE ANTENNA

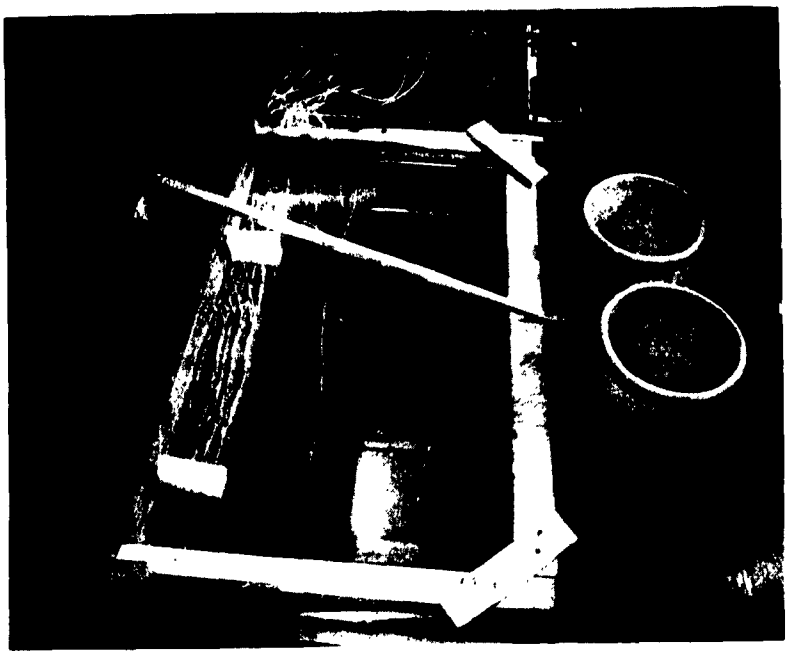

FIG. 3-21 PHOTO OF THE STRATIFIED LAYERS IN THE TANK

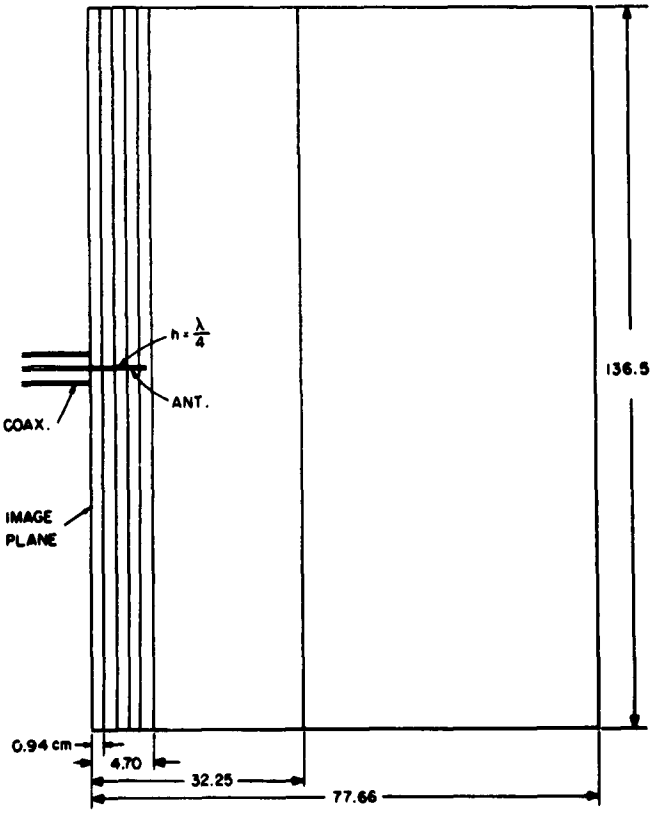

FIG. 3-22 DIMENSION OF THE STRATIFICATION OF THE TANK

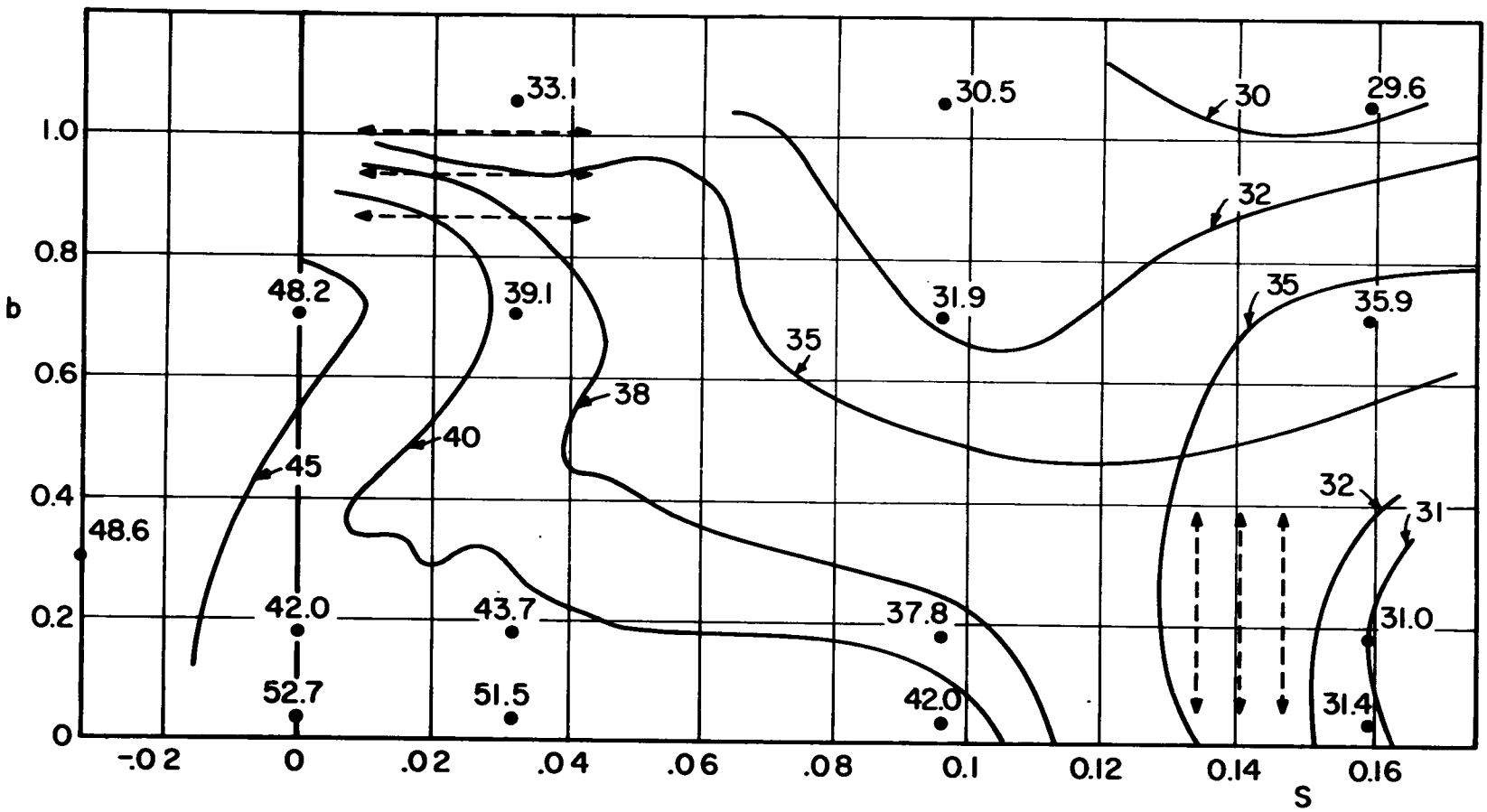

FIG. 3-23 EQUI-CONDUCTANCE LINE FOR A HALF-WAVE DIPOLE ANTENNA IN THE STRATIFIED MEDIUM.

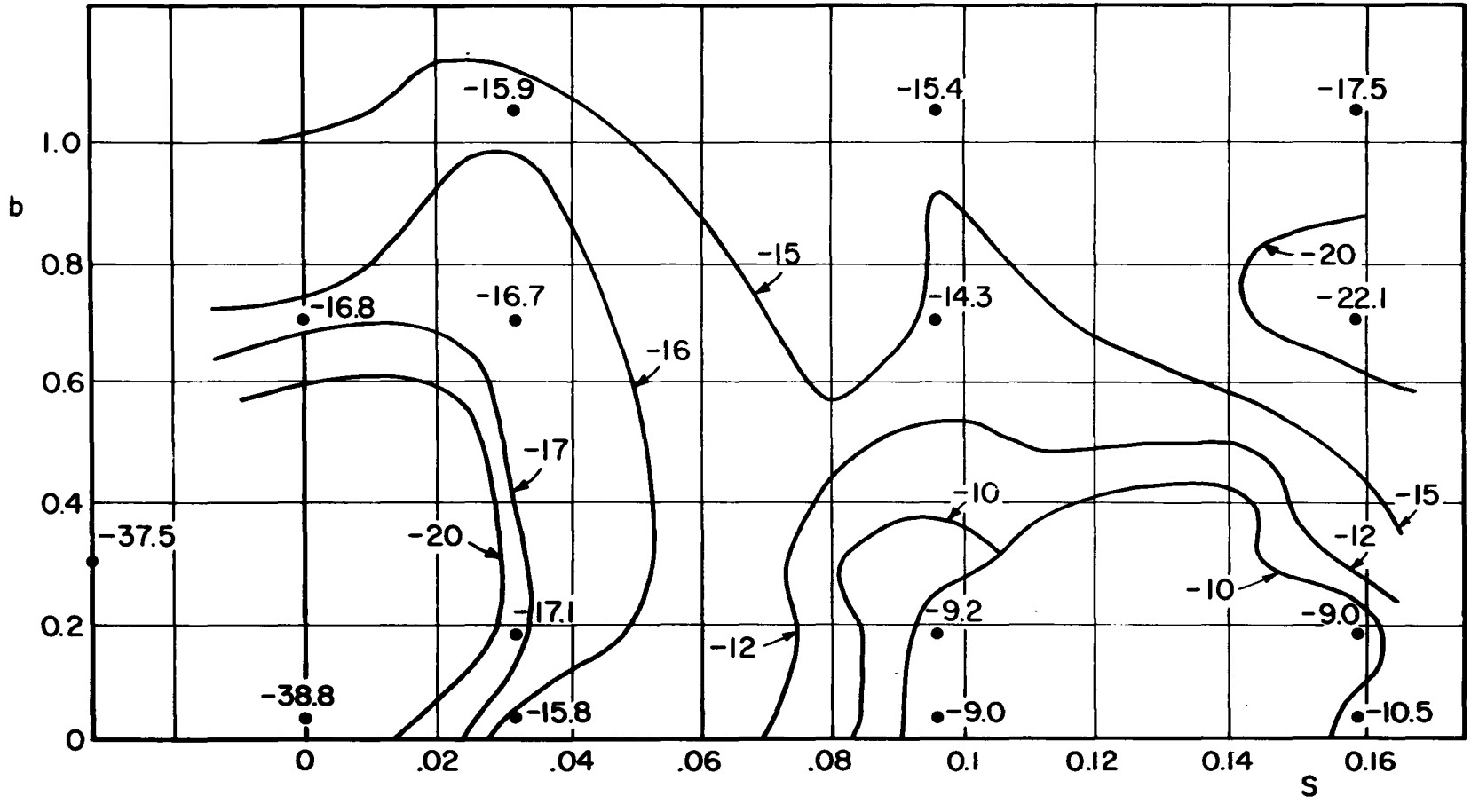

FIG. 3-24 EQUI-SUSCEPTANCE LINE FOR A HALF-WAVE DIPOLE ANTENNA IN THE STRATIFIED MEDIUM.

The conductance and the absolute value of susceptance both have the largest value at the origin; both of these values are largest with a homogeneous medium of the lowest conductivity and any change from homogeneity gives rise to a decrease in both the driving-point conductance and in the absolute value of the susceptance. It may be added that this property of a half-wave dipole antenna could well be applied to the detection of an inhomogeneity in a medium (or material).

For a fixed value of b, the conductance and the absolute value of the susceptance always decrease with an increase in S values. (The reverse statement is not quite true.) As a more general trend, the direction of the contours of constant conductance more or less follow the broken lines in the figures. This means that for the smaller values of b, a change in S has more effect on the conductance than does a change in b. For the smaller values of S the situation is reversed and a change in b has more effect on the conductance than does a change in S.

Current Distribution

The amplitude and phase distributions of the current were measured for a half-wave dipole antenna in the stratified medium with the same configurations mentioned in the preceding section. The combination of b and S values is the same as is tabulated in Table 3-11. The measured results are normalized in the same way as mentioned above and are plotted in Figs. 3-25 through 3-29. The conductivity associated with distribution of current is indicated in the same figures. For better comparison the curves for the same b values are also plotted on the graphs. It is observed that the amplitude of the current $|I|/V$ along the antenna with larger S values for a fixed b value is always smaller than the current distribution with smaller S values. The in-phase component I''/V and quadrature component I'/V of the current also follow this general rule. The general shapes of the distributions of current, however, stay practically the same for all of the various combinations of b and S.

With an increase in the value of S for a fixed b, the slope of the curve θ_I with respect to the position along the antenna becomes steeper.

It is more difficult to make a general statement about changes in S for a fixed value of b , but with some exceptions the above-mentioned statement holds if b is substituted for S and vice versa.

Conclusions

The experimental measurements were made with both homogeneous and inhomogeneous media.

A. Results with a Homogeneous Medium

(1) The driving-point admittance was measured for the range from $\beta h = 0.1$ to $\beta h = 2\pi$ at intervals of $\beta h = 0.1$. The properties of the solution were varied from $\epsilon_r = 78$ $\sigma/\omega\epsilon_r\epsilon_o = 0.036$ to $\epsilon_r = 69$ $\sigma/\omega\epsilon_r\epsilon_o = 8.8$. A general characteristic of the curves shows that not only the size of the spiral curves on the admittance chart becomes smaller but also the convergence of the spiral with respect to βh becomes faster as $\sigma/\omega\epsilon_r\epsilon_o$ is increased.

(2) The point of convergence of the spiral moves from the capacitive region into the inductive region with an increase in $\sigma/\omega\epsilon_r\epsilon_o$.

(3) All loci of the admittance with an increase in $\sigma/\omega\epsilon_r\epsilon_o$ except for antennas shorter than $\beta h = \pi/2$ first meet near the point of the characteristic admittance of the coaxial line. The loci from the meeting point on are practically the same regardless of the length of the antenna. From this fact the following generalized statements have been established :

(a) The loci almost without exception select the shortest path to the meeting point.

(b) As a consequence of (a) the shape of the driving-point admittance with respect to the conductivity of the solution could be classified in four groups depending on the length of the antenna.

(4) The condition of resonance does not occur when the length of the antenna exceeds $\beta h = \pi$ in the solution of higher conductivities.

(5) The resonance points, if any, shift toward the origin as $\sigma/\omega\epsilon_r\epsilon_o$ is increased.

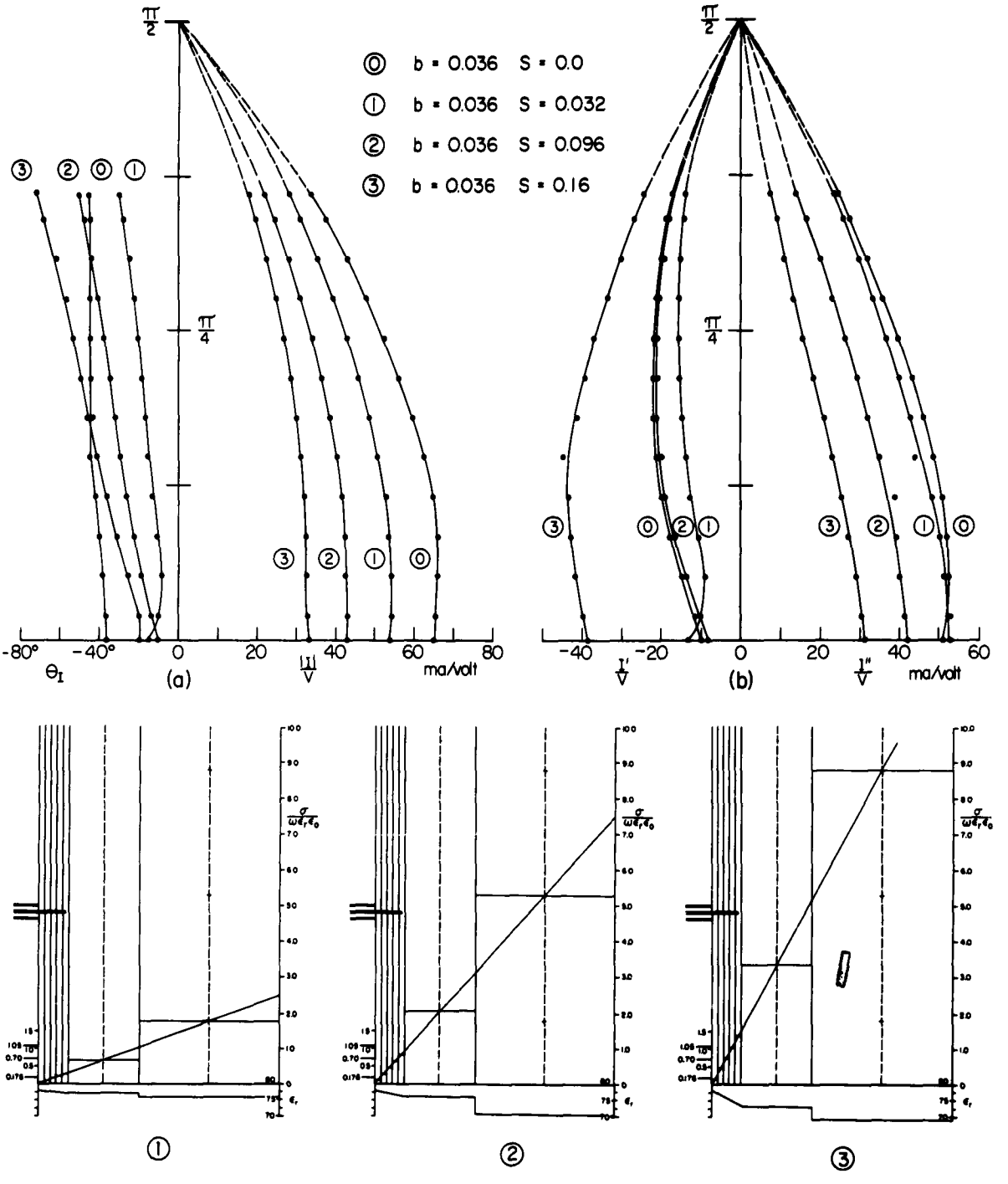

FIG. 3-25 (a) NORMALIZED CURRENT $\frac{I}{V} = \frac{|I|}{V} e^{j\theta_I}$ IN STRATIFIED MEDIA WITH $b = 0.036$ $\left[\frac{\sigma}{\omega \epsilon_r \epsilon_0} = b + SX\ (CM)\right]$

(b) NORMALIZED CURRENT $\frac{I}{V} = \frac{I''}{V} + j\frac{I'}{V}$ IN STRATIFIED MEDIA WITH $b = 0.036$

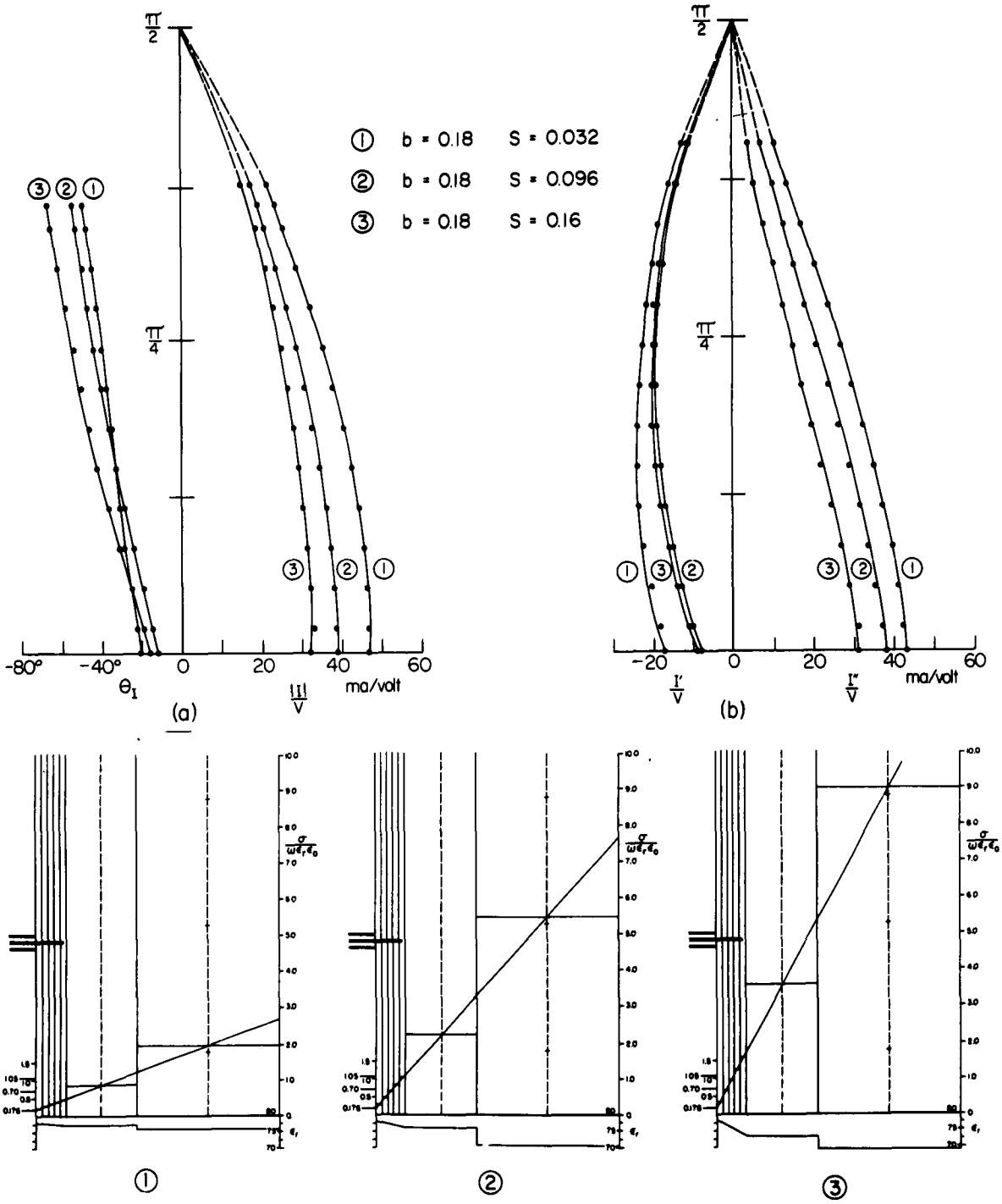

FIG 3-26 (a) NORMALIZED CURRENT $\frac{I}{V} = \frac{|I|}{V} e^{j\theta_I}$ IN STRATIFIED MEDIA WITH $b = 0.18$ $\left[\frac{\sigma}{\omega \epsilon_r \epsilon_0} = b + SX\ (CM)\right]$

(b) NORMALIZED CURRENT $\frac{I}{V} = \frac{I''}{V} + j\frac{I'}{V}$ IN STRATIFIED MEDIA WITH $b = 0.18$

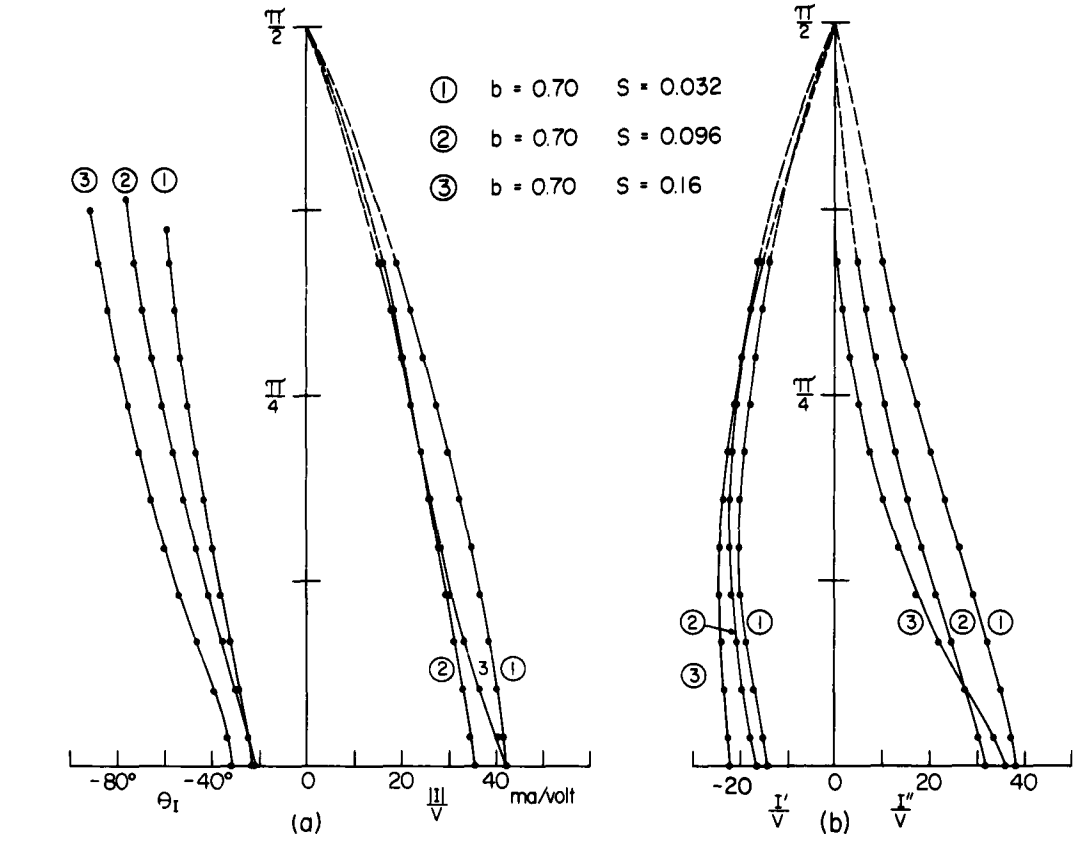

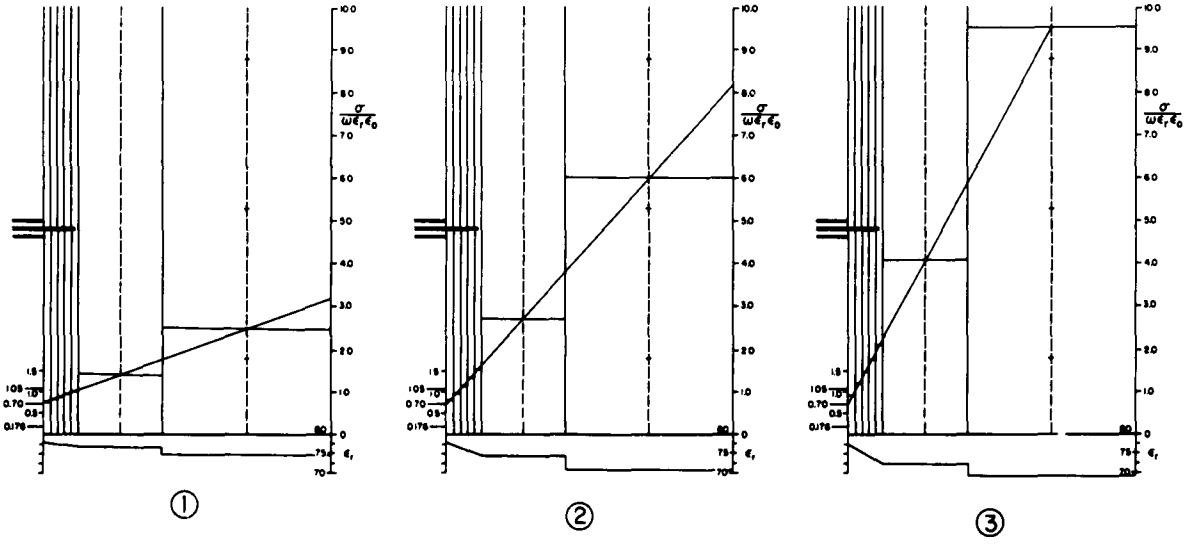

FIG 3-27 (a) NORMALIZED CURRENT $\frac{I}{V} = \frac{|I|}{V} e^{j\theta_I}$ IN STRATIFIED MEDIA WITH $b = 0.70$ $\left[\frac{\sigma}{\omega \epsilon_r \epsilon_0} = b + SX\ (CM)\right]$

(b) NORMALIZED CURRENT $\frac{I}{V} = \frac{I''}{V} + j\frac{I'}{V}$ IN STRATIFIED MEDIA WITH $b = 0.70$

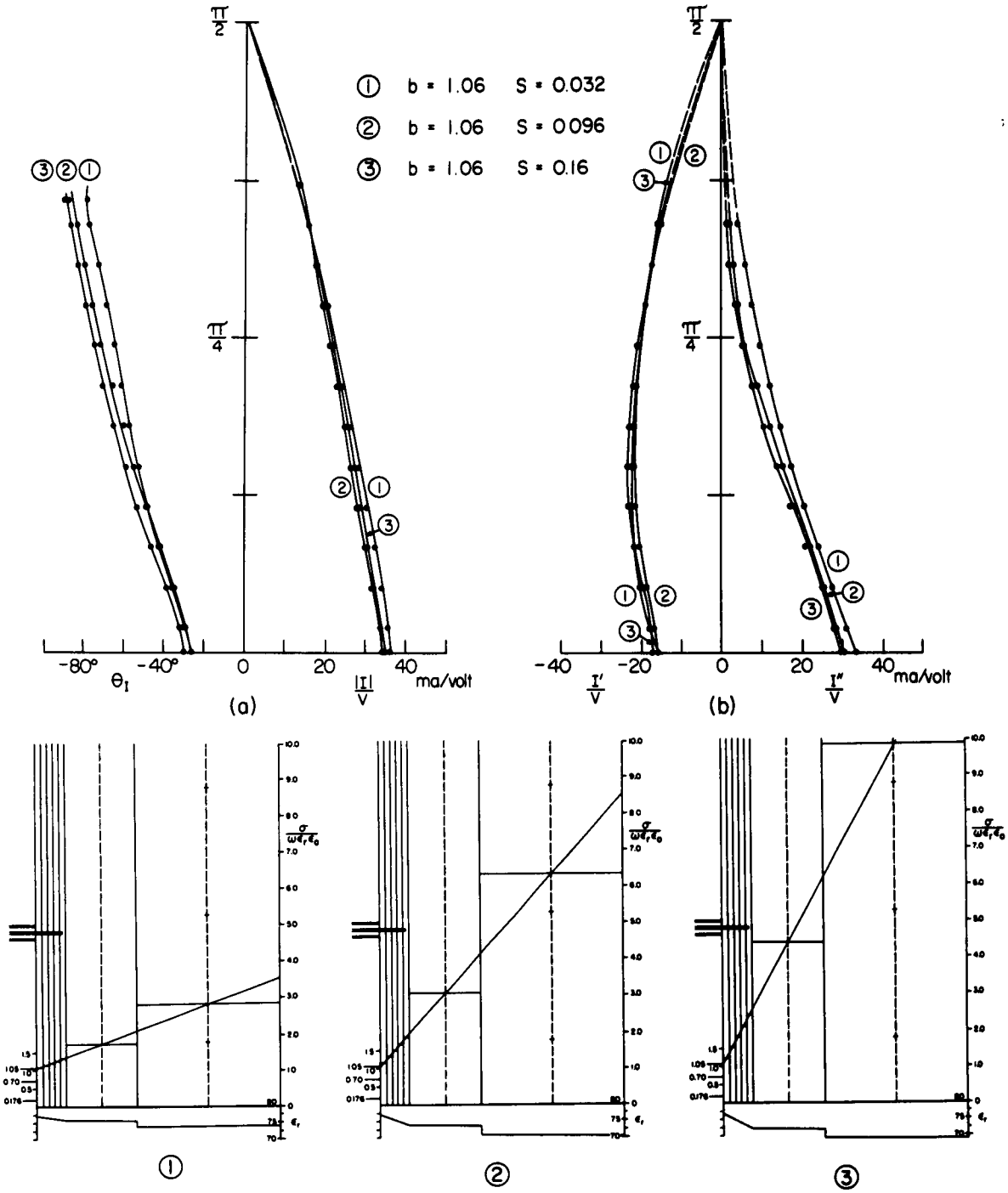

FIG 3-28 (a) NORMALIZED CURRENT $\frac{I}{V} = \frac{|I|}{V} e^{j\theta_I}$ IN STRATIFIED MEDIA WITH $b = 1.06$ $\left[\frac{\sigma}{\omega \epsilon_r \epsilon_0} = b + SX\ (CM)\right]$

(b) NORMALIZED CURRENT $\frac{I}{V} = \frac{I''}{V} + j\frac{I'}{V}$ IN STRATIFIED MEDIA WITH $b = 1.06$

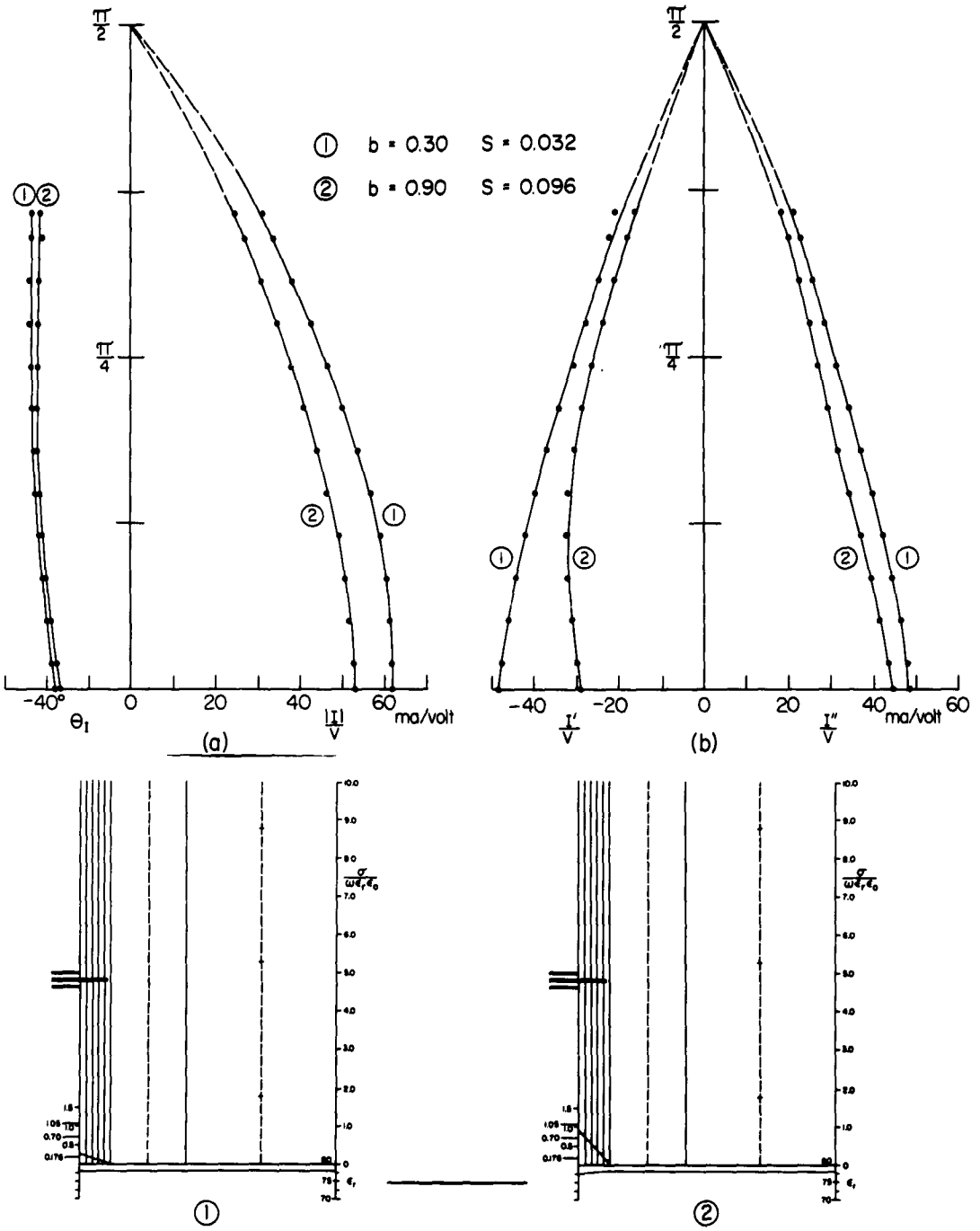

FIG 3-29 (a) NORMALIZED CURRENT $\frac{I}{V} = \frac{|I|}{V} e^{j\theta_I}$ IN STRATIFIED MEDIA WITH $b = 0.30$, $b = 0.90$ $\left[\frac{\sigma}{\omega \epsilon_r \epsilon_0} = b + SX\ (CM)\right]$

(b) NORMALIZED CURRENT $\frac{I}{V} = \frac{I''}{V} + j\frac{I'}{V}$ IN STRATIFIED MEDIA WITH $b = 0.30$, $b = 0.90$

(6) Both the distribution of current and the admittance for antennas with $\beta h = 0.3$ and $\beta h = \pi/2$ are in fair agreement with the theoretical results obtained by R. W. P. King and C. W. Harrison.

(7) The current distributions change from concave outward to concave inward as $\sigma/\omega\epsilon_r\epsilon_o$ is increased.

(8) The shape of the in-phase component of current, in general, exhibits a greater change in curvature than does the shape of the quadrature component.

(9) The curve of the phase θ_I becomes more like that of a traveling wave antenna with an increase in conductivity.

(10) The current distributions on short antennas become very close to the shape of a triangle at high conductivity of the solution.

B. Results with an Inhomogeneous Medium

(1) Differences in admittance with and without the partition film were measured to be less than 7 ~ 8 percent.

(2) The driving-point admittance was measured for various combinations of b and S values of the conductivity where $\sigma/\omega\epsilon_r\epsilon_o = b + Sx$.

(3) Both conductance and susceptance have the largest value at the origin of the b - S equi-admittance curves. This property might be applied to the detection of an inhomogeneity in a medium.

(4) For a fixed value of b, the values of G and $|B|$ always decrease with an increase in S values.

(5) For smaller values of b, a change in the S value has a greater effect on the admittance than a change in the b value, and for smaller values of S, the change in b has a greater effect on the admittance than a change in S.

(6) Values of $|I|/V$, I''/V, and I'/V along the antenna with larger S values (for a fixed b) are smaller than those with smaller S values.

(7) The curve of 0 has a steeper slope with larger S values for a fixed b value.

IV. Miscellaneous

1. Change of Admittance Due to the Local Change of the Properties of Medium.

If the dipole antenna is used as a probe to determine the local properties of a medium or the spatial distribution of the properties of a medium, it is desirable to know the distance beyond which a change in the properties of the medium has no effect on the driving-point admittance of the antenna. Accordingly, the driving-point admittance of a half-wave dipole was measured as a function of the conductivity of a part of the medium in the suitably partitioned tank which has already been described in the previous section (see Fig.3-22).

The geometric distribution of the conductivity of the partitioned medium and the corresponding measured driving-point admittances are all listed in Fig. 4 - 1. The driving-point admittance of the antenna in a medium which is homogeneous with $\frac{\sigma}{\omega\epsilon_r\epsilon_0} = 0.036$ except for the presence of six partitioning films was measured to be $Y = 53.2 - j36.7$ (millimhos).

The deviations ΔY of the driving-point admittance from the above value for the homogeneous case are also shown in the figure. The conductivities of the solution in the several compartments are in Table 4 - 1.

Compartment No. / Fig. No.	No. 1	No. 2	No. 3	No. 4	No. 5	No. 6	No. 7
a							1.76
b						0.665	1.76
c					0.271	0.665	1.76
d					0.271	0.665	1.94
e					0.271	0.841	1.94
f					0.447	0.841	1.94
g				0.385	0.447	0.841	1.94
h			0.326	0.385	0.447	0.841	1.94
i		0.266	0.326	0.385	0.447	0.841	1.94
j	0.206	0.268	0.326	0.385	0.447	0.841	1.94

Blank Columns are $\frac{\sigma}{\omega\epsilon_r\epsilon_0} = 0.036$

Table 4-1 Distribution of $\frac{\sigma}{\omega\epsilon_r\epsilon_0}$ in the Compartments.

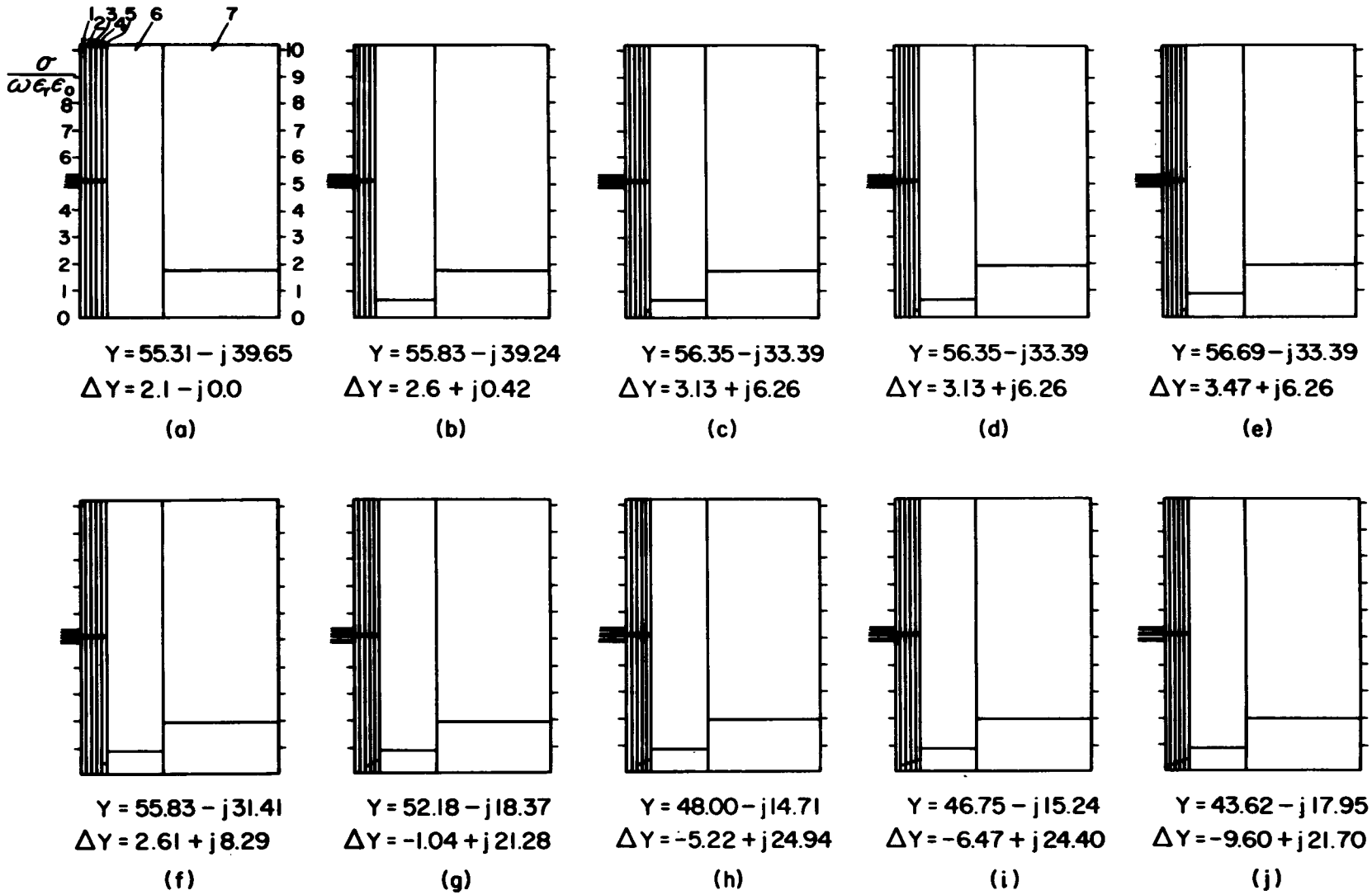

FIG. 4-1 ADMITTANCE OF HALF-WAVE DIPOLE ANTENNA IMMERSED IN INHOMOGENEOUS MEDIA

The conductivity of the solution in the seventh compartment (which is the farthest from the antenna - its boundary with the sixth compartment is about $^3/_4$ λ away), was increased gradually until a change in the admittance of the antenna was observed. The conductivities of all other compartments were kept at $\frac{\sigma}{\omega\epsilon_r\epsilon_0} = 0.036$, (see Fig. 4-1(a)). The conductivity of compartment No. 7, at which the admittance became apparent was $\frac{\sigma}{\omega\epsilon_r\epsilon_0} = 1.76$. This initial change occurred in the conductance, not in the susceptance, that is $\Delta Y = 2.1 - j0.0$.

Next, the conductivity of the solution in the sixth compartment was increased to $\frac{\sigma}{\omega\epsilon_r\epsilon_0} = 0.665$. The conductivity of the seventh compartment was kept the same as in case (a). This time slight increases in both conductance and susceptance were detected simultaneously, i.e., $\Delta Y = 2.6 + j0.42$.

In case (c) the conductivity of the sixth and the seventh compartments were kept as in case (b) and the conductivity of the fifth compartment alone was raised to $\frac{\sigma}{\omega\epsilon_r\epsilon_0} = 0.27$. The observed change in admittance is rather large, especially that of susceptance. It can be seen that as soon as a change is made in the conductivity of a compartment which contains a part of the antenna in direct contact with the solution, the admittance of the antenna is affected greatly. (Note that the boundary between the fifth and sixth compartments is only $\lambda/40$ away from the tip of the antenna.)

When the conductivity in the seventh compartment was further increased to $\frac{\sigma}{\omega\epsilon_r\epsilon_0} = 1.94$ (see (d)), no change in admittance was observed. When the ratio $\frac{\sigma}{\omega\epsilon_r\epsilon_0}$ of the solution in the sixth compartment was increased from 0.665 in case (d) to 0.841 in case (e) with no change in the other compartments, a slight difference in conductance was observed but no change in susceptance. It appears that when a part of the antenna is in direct contact with the conducting solution and the conduction current from this part into the solution is not greatly disturbed, the antenna becomes quite insensitive to changes in the conductivity of the solution which is not in direct contact with the antenna.

The conductivity of the fifth compartment was almost doubled to obtain the conditions of case (f) from those of case (e). As a result ΔG began to decrease, ΔB to increase. In the cases (g), (h), and (i), the conductivities in the smallest compartments were increased successively until the final configuration (j) was reached for which the conductivity of the solution increases stepwise from

layer to layer, and the geometric centers of each layer follow the straight line characterized by $b = 0.206$ and $S = 0.032$ in the formula $\frac{\sigma}{\omega \epsilon_r \epsilon_o} = b + Sx$ (x in cm). It is to be noted that ΔG decreases progressively and ΔB progressively increases.

Further conclusions are not possible from the available experimental data, so that a more extensive systematic study is indicated.

2. Stratification of the Medium to Achieve a Gradient of the Dielectric Constant.

Acetonitrile CH_3CN was mixed with water in order to vary the dielectric constant of the solutions in the several compartments of the tank. A description of the properties of CH_3CN are found in Scientific Report No. 1.[4]

Since acetonitrile is flammable (flash point is 55°F - approximately that of methyl alcohol) and toxic (maximum allowable concentration for continuous exposure - 8 hours per day, five days per week - is 20 parts of acetonitrile vapor per million parts of air,[5]) it was necessary to take special precautions in handling the solution. A platform (see Fig. 4-2) about two feet above the top surface of the tank was constructed outside the room so that the transfer of acetonitrile from the drum to the tank could be accomplished by gravity feed. The gravity feed was preferred in order to avoid any possible ignition hazard with the electric motor-driven pump.

Metal hoses were used in order to avoid a possible ignition hazard from static electricity generated by the flow of the non-conducting liquid from the drum through pipes to the tank.

In order that the concentration of acetonitrile could be kept below 20 ppm in the experimenters' breathing area, an enclosing hood (Fig. 4-3) was installed over the tank. The lower front edge of the cover is cut out for the air intake; the back of the hood is attached to a four-inch exhaust pipe which is connected to a 1/3 HP explosion-proof motor that blows the fumes from the surface of the tank to the outdoors.

Experimental data are available for only one configuration of a stratified medium into layers with different dielectric constants. It is represented in Table 4-2 and Fig. 4-4.

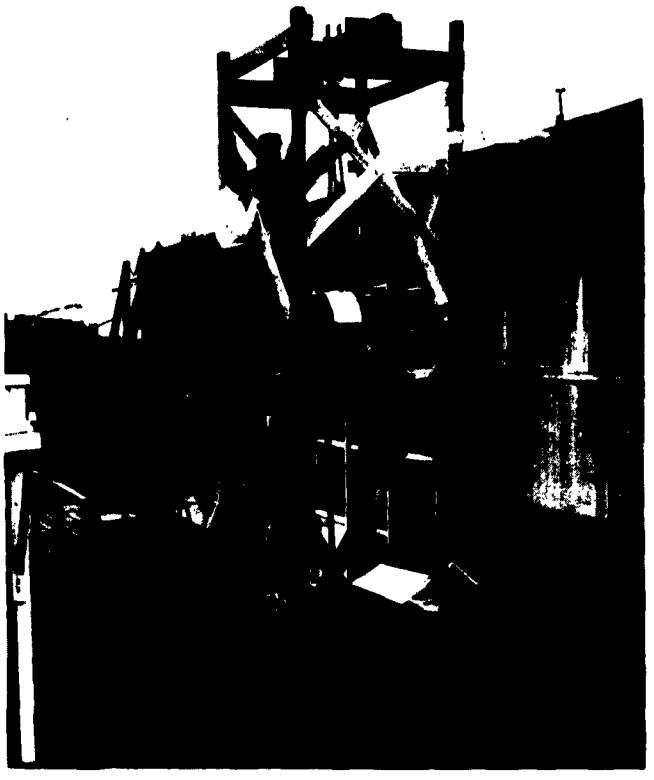

FIG. 4-2

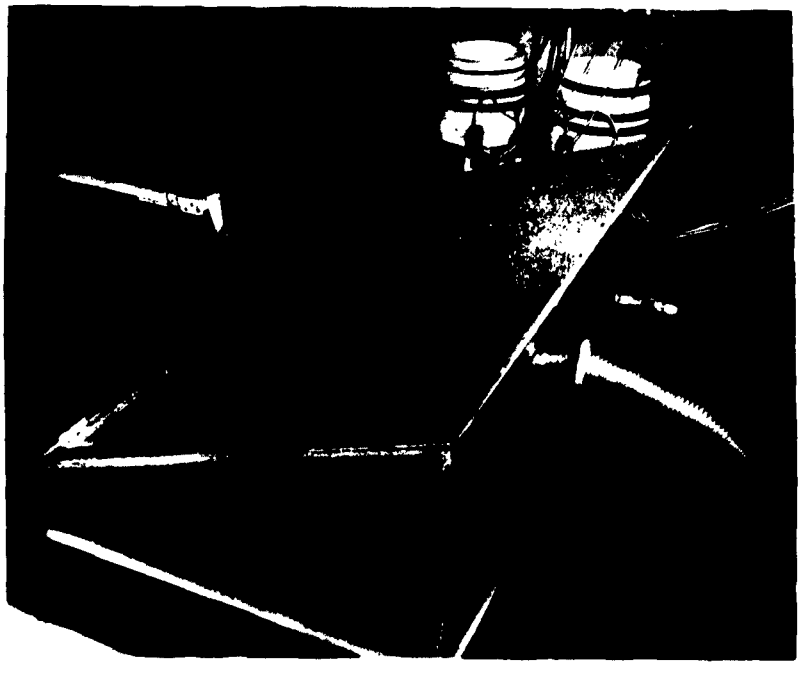

FIG. 4-3

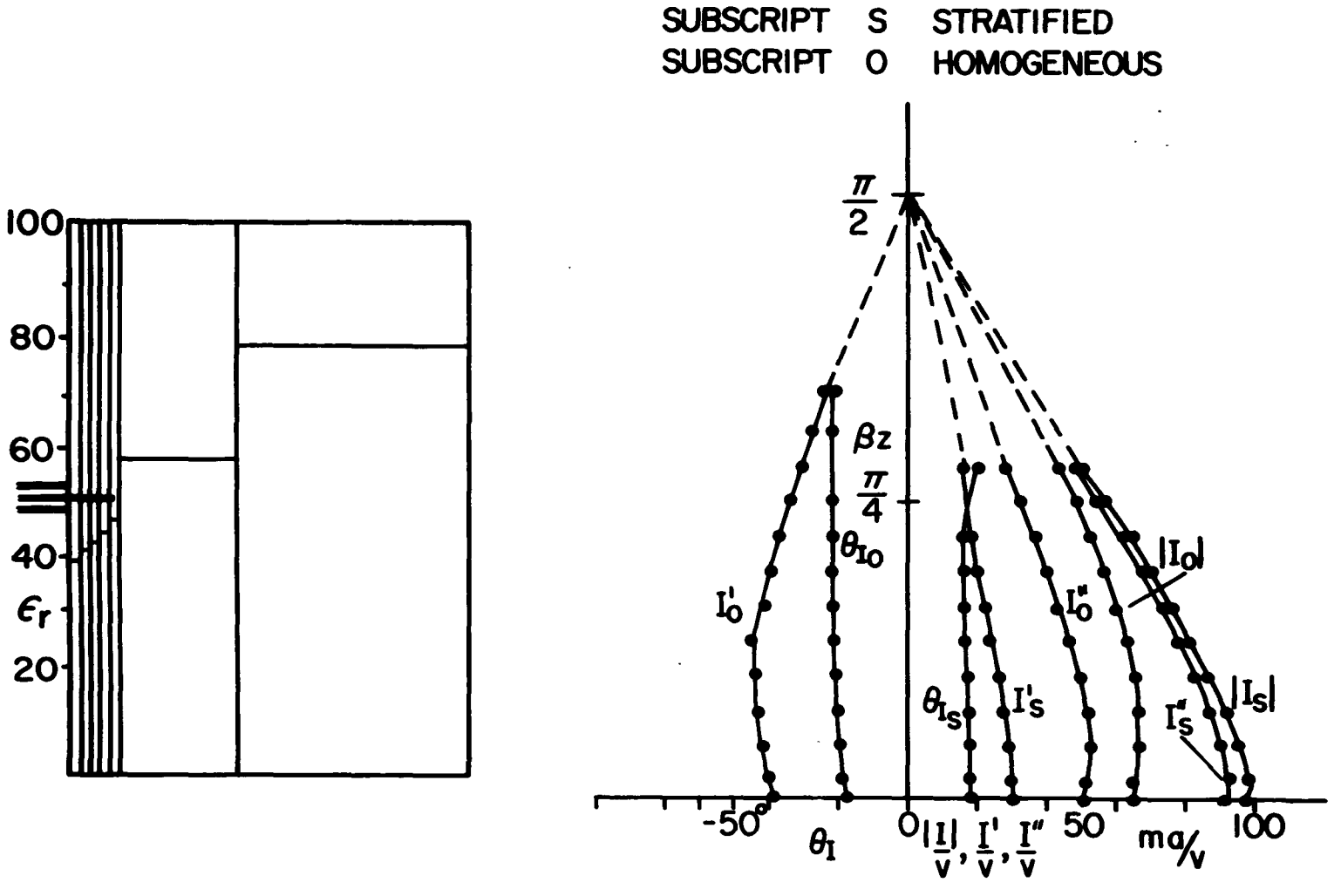

FIG. 4-4 CONFIGURATION OF STRATIFICATION AND CURRENT DISTRIBUTION ON THE ANTENNA

Table 4 - 2

Compartment No.	Relative Dielectric Constant
1	38.5
2	41.0
3	42.2
4	44.0
5	46.3
6	57.8
7	78.0

The current distributions on a half-wave antenna when immersed in the stratified medium and in a homogeneous medium with $\epsilon_r = 78$ and $\frac{\sigma}{\omega \epsilon_r \epsilon_o} = 0.036$ are also shown in Fig. 4-4. The length h of the antenna in the stratified medium was one-quarter of a wavelength in the medium of $\epsilon_r = 78$ and $\frac{\sigma}{\omega \epsilon_r \epsilon_o} = 0.036$. The current along the antenna is normalized in the same way as in the previous section.

Since data for only one case are available, it is not possible to draw definitive conclusions. The shape of the current distribution for the antenna in the stratified medium is more triangular than sinusoidal. With reference to Fig. 3-19' , it is clear that the distribution of current along the antenna in the stratified medium behaves more like that along an antenna in a dissipationless medium with $\beta h = \frac{\pi}{4}$ than with $\beta h = \frac{\pi}{2}$. The curve of the angle θ_{I_s} is seen to be positive as is that for θ when $\beta h = \frac{\pi}{4}$ in a medium with $\epsilon_r = 78$. The measured driving-point admittance in this stratified case is

$$Y = 91.26 + j34.23 .$$

With reference to the Figs. 3-12 and 3-13, this admittance is seen to be rather close to that of an antenna in a dissipationless medium with $\beta h = 1.2$ in both real and imaginary parts. This is just as if the wavelength in the medium had been increased by a factor $\frac{\lambda_s}{\lambda_{78}} = \frac{1.57}{1.20} = 1.31$ or $\lambda_s = 1.31 \lambda_{78}$, or as if the antenna whose electrical length βh is $\frac{\pi}{2}$ in a solution with $\epsilon_r = 78$ were immersed in a homogeneous dielectric medium whose dielectric constant is $\epsilon_{eff} = 78 \left(\frac{\lambda_{78}}{\lambda_s}\right)^2 = 45.5$.

3. Driving-point Admittance of a Dipole Antenna Coated with a Cylinder of Square Cross Section.

A wooden rectangular cylinder was installed across the tank from the image plane to the back wall of the tank. The antenna was placed along the center line of the rectangular cylinder.

The cylinder was filled with the solution of acetonitrile ($\epsilon_r = 38.5$); outside the cylinder was air. The cross section of the cylinder was square with the side dimension $\frac{D}{\lambda} = 0.295$ and thickness of the wooden wall $\frac{d}{\lambda} = 0.0107$.

The driving-point admittance was measured for the range from $\frac{2\pi}{\lambda} h = 0.35$ to $\frac{2\pi}{\lambda} h = 4.41$ where λ is the wavelength inside a homogeneous solution with $\epsilon_r = 38.5$. The measured results are plotted in Fig. 4-5 on a rectangular admittance chart with the length of the antenna $\frac{2\pi}{\lambda} h$ as the parameter. The resonant length is $\beta h = 2.53$ which is about one and a half times longer than when the antenna is immersed in an infinite homogeneous medium with $\epsilon_r = 38.5$.

The diameter of the spiral is about 45 millimhos; that is, about three times as large as that for free space and about one-half that of the antenna immersed in a homogeneous medium of $\epsilon_r = 38.5$.

The spirals of admittance for the case of free space ($\epsilon_r = 1$) and in a homogeneous dielectric with $\epsilon_r = 38.5$ are shown in broken lines in the same figure.

Since the size of the present image plane may be somewhat small for accurate measurements when the medium is dissipationless, the results should not be regarded as definitive.

More complete and more systematic experiments should follow the present preliminary and exploratory series.

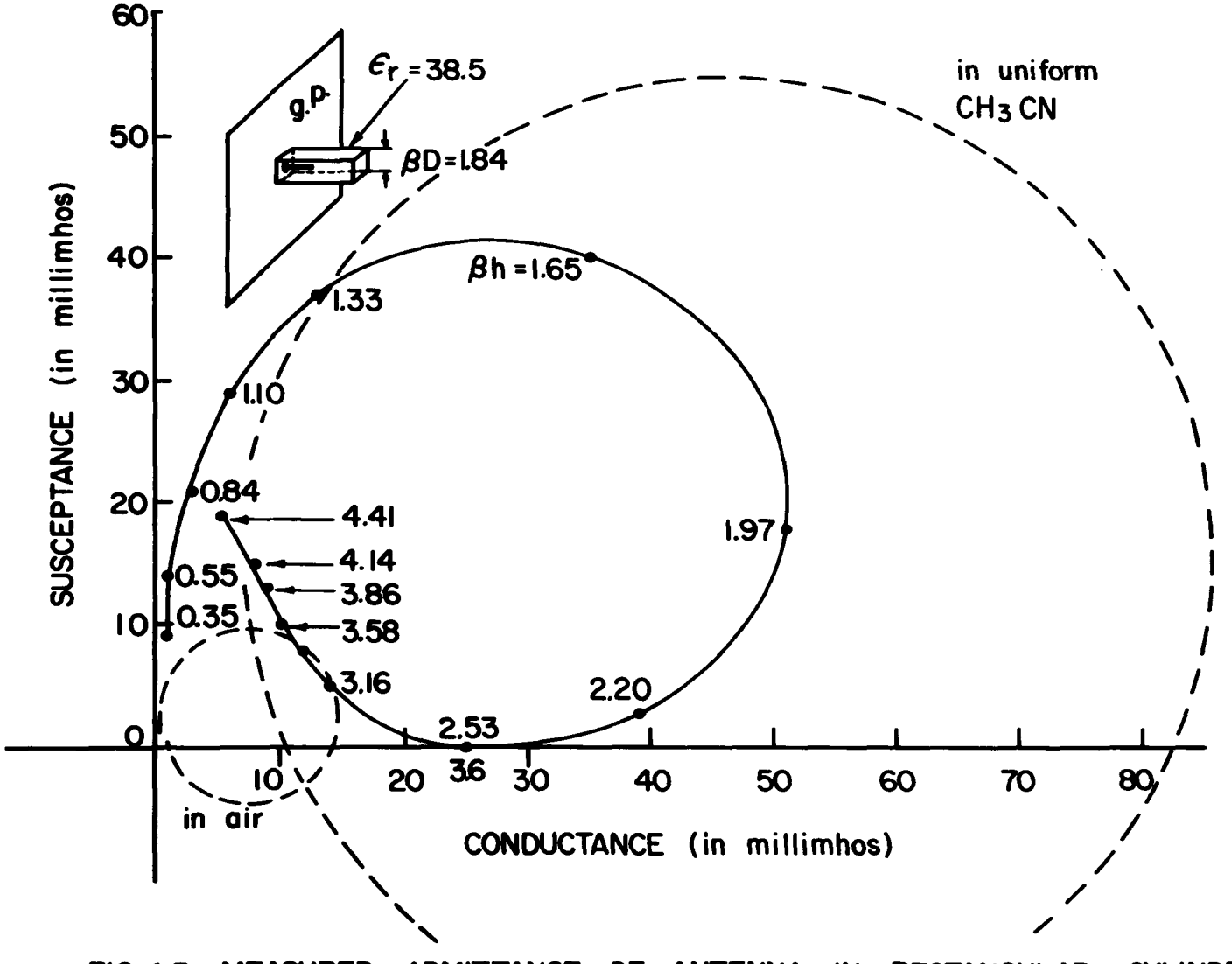

FIG. 4-5 MEASURED ADMITTANCE OF ANTENNA IN RECTANGULAR CYLINDER

Acknowledgements

The authors wish to express their appreciation to Mr. Donald J. Mac Millan who was responsible for the construction of the apparatus, Mr. Stéphane Prévot who assisted in arranging the electronic equipment, Miss Dilla W. Gooch who helped with the stratification of the tank, and to Miss Ruth Edelson and her assistants who reduced the data.

They also wish to thank Messrs. William A. Burgess and Frank A. Lawton for their deep concern with the safe handling of acetonitrile.

References

1. King, R. W. P., "Dipoles in Dissipative Media", Cruft Laboratory Technical Report No. 336, Harvard University, February 1961.
2. Altshuler, E. E., "The Traveling - Wave Linear Antenna", Cruft Laboratory Scientific Report No. 7, Harvard University, May 1960.
3. King, R. W. P. and Harrison, C. W. Jr., "Half-Wave Cylindrical Antenna in a Dissipative Medium; Current and Impedance", J. Research of N.B.S. 640 1960, pp. 365 - 380.
4. Iizuka, K. and King, R. W. P., "Apparatus for the Study of the Properties of Antennas in a Conducting Medium", Cruft Laboratory Scientific Report No. 1, May 1961.
5. Burgess, William A., from private communication.

Science Advisor
Department of State
Washington 25, D. C.

Office of Secretary of Defense
(DDR+E, Tech. Library)
Washington 25, D. C.

Institute of Technology Library
MCLI-LIB, Bldg. 125, Area B
Wright-Patterson Air Force Base, Ohio

Hq. USAF (AFCSA, Secretary)
Washington 25, D. C.

Hq. USAF (AFRDR)
Washington 25, D. C.

AFCRL, OAR(CRIPA) Stop 39
L. G. Hanscom Field [20]
Bedford, Massachusetts

ESD(ESRDG)
L. G. Hanscom Field
Bedford, Massachusetts

Boston Office
Patents + Royalties Div. (Hq. AFLC)
Bldg. 133, 424 Trapelo Road
Waltham 54, Massachusetts

ASD (ASAPRD-Dist)
Wright-Patterson AFB, Ohio

ACIC (ACDEL-7)
2d + Arsenal
St. Louis 18, Missouri

NAFEC Library Branch, Bldg. 3
Atlantic City, New Jersey
Attn: RD-702

AFCRL, OAR (CRT, Dr. A. M. Gerlach)
L. G. Hanscom Field
Bedford, Massachusetts

OAR (RROS) Bldg. T-D
Washington 25, D. C.

Dr. R. Jastrow
NASA Goddard Space Flight Center
Washington 25, D. C.

NASA
Attn: Library, Code AFET-LA
Stop 85
Washington 25, D. C.

Librarian
Boulder Laboratories
National Bureau of Standards
Boulder, Colorado

Library
National Bureau of Standards
Washington 25, D. C.

Director of Meteorological Research
U. S. Weather Bureau
Washington 25, D. C.

Library
U. S. Weather Bureau
Suitland, Maryland

Director, USAF Project RAND
The Rand Corporation
1700 Main Street
Santa Monica, California
Thru A. F. Liaison Office

Dr. William W. Kellogg
Rand Corporation
1700 Main Street
Santa Monica, California

Mr. Malcolm Rigby
American Meteorological Society
P. O. Box 1736
Washington 13, D. C.

Institute of Aerospace Sciences, Inc.
2 East 64th Street
New York 21, New York

Professor E. C. Jordan
Electrical Engineering Dept.
University of Illinois, Urbana, Illinois

Mr. Warren W. Berning
Ballistic Research Laboratories
Aberdeen Proving Ground, Maryland

AFCRL, OAR(CRIP, Mr. J. Marple)
L. G. Hanscom Field
Bedford, Massachusetts

AFOSR (SRQL)
Washington 25, D. C.

AWS (AWSSS/TIPD)
Scott AFB, Illinois

A. U. (Library)
Maxwell AFB, Alabama

Department of the Army(SIGRD-8-B-5)
Washington 25, D. C.

Technical Documents Center
Evans Signal Laboratories
Belmar, New Jersey

Technical Reports Librarian
U. S. Naval Postgraduate School
Monterey, California

Director
U. S. Naval Research Laboratory
Code 2027
Washington 25, D. C.

ONR(Geophysics Code N-416)
Office of Naval Research
Washington 25, D. C.

Documents Expediting Project (UNIT X)
Library of Congress
Washington 25, D. C.

Superintendent of Documents
Government Printing Office
Washington 25, D. C.

ASTIA (TIPAA) [10]
Arlington Hall Station
Arlington 12, Virginia

National Research Council
2101 Constitution Ave.
Washington 25, D. C.

Professor S. F. Singer
Department of Physics
University of Maryland
College Park, Maryland

Dr. S. A. Bowhill
Ionospheric Research Laboratory
Pennsylvania State University
University Park, Pennsylvania

Library
Geophysical Institute
University of Alaska
P. O. Box 938
College, Alaska

Dr. Joseph Kaplan
Department of Physics
University of California
Los Angeles, California

Prof. Fred L. Whipple
Harvard College Observatory
60 Garden Street
Cambridge 38, Massachusetts

Dr. David Fults
Department of Meteorology
University of Chicago
Chicago, Illinois

Dr. A. M. Peterson
Stanford University
Stanford, California

Professor Clarence Palmer
Institute of Geophysics
University of California
Los Angeles 24, California

Technical Information Office
European Office, Aerospace Research
Shell Building, 47 Cantersteen
Brussels, Belgium

Professor H. G. Booker
School of Electrical Engineering
Cornell University
Ithaca, New York

Dr. P. R. Arendt
U. S. Army Signal R+D Laboratory
Fort Monmouth, New Jersey

*One copy, unless specified otherwise by numbers enclosed in brackets.